IEEE Access
Multidisciplinary | Rapid Review | Open Access Journal

Received December 9, 2021, accepted December 16, 2021, date of publication December 20, 2021,
date of current version December 27, 2021.

Digital Object Identifier 10.1109/ACCESS.2021.3136713

Wind Turbine Oriented Solutions to Improve Power Quality and Harmonic Compliance of AC Offshore Wind Power Plants

CARLOS RUIZ[1], GONZALO ABAD[1], MARKEL ZUBIAGA[2], DANEL MADARIAGA[2], AND JOSEBA ARZA[2]

[1]Electronics and Computer Science Department, Mondragon University, 20500 Mondragon, Spain
[2]Ingeteam Research and Development Europe S. L., 48170 Zamudio, Spain

Corresponding author: Carlos Ruiz (cruiz@mondragon.edu)

ABSTRACT The operation of offshore wind power plants with respect to power quality and grid code compliance must be verified for different conditions in the design phase using harmonic analysis methods. This paper addresses this verification by first considering a scenario in which wind turbines operate with a typically used modulation strategy, carrier-based pulse width modulation. The studies are performed at several operating points, not only at the rated condition, and at two points of the electrical infrastructure, at the point of connection of the wind turbine and at the point of common coupling of the offshore wind farm. For this type of modulation technique and according to the resonance conditions of the studied offshore system, the harmonic distortion of current signals is relatively high and the compliance of the German – grid code is not achieved. To tackle this, wind turbine manufacturer oriented solutions are proposed with the aim of improving the harmonic emission of the offshore wind farm. The implementation of a particular solution of selective harmonic elimination is presented together with complementary solutions to further improve the harmonic emission of the wind power facility. Furthermore, this paper discloses the modeling approach to account for an adequate harmonic assessment of the wind power plant under study.

INDEX TERMS Wind energy integration, offshore wind power plants, power system harmonics, power harmonic filter, grid code, modulation strategies.

I. INTRODUCTION

Harmonics are a special concern in the offshore wind industry due to the high penetration of power converters in type-4 wind turbines [1].

Type-4 wind turbines (WTs) offer many advantages, which is why they are installed in offshore wind power plant (OWPP) scenarios. Some examples of these advantages are increased power extraction efficiency, voltage- and frequency support, and fault ride-through (FRT), which are provided by means of proper control of the power converter [2].

Despite the previous advantages, type-4 WTs can be considered as a source of harmonics, which significantly contributes to the overall harmonic emission at the point of common coupling (PCC) of the OWPP. Furthermore, this contribution can be worsened due to the presence of resonances that may increase a given voltage- or current-harmonic component. These resonances can be classified into series- and parallel resonances and they occur due to capacitive (submarine cables) and inductive (transformer) behavior of installed power components in combination with the impedance of the grid.

Maximum harmonic injection limits of voltage- and current-signals are commonly imposed by grid codes and interconnection agreements [3], [4]. These limits are typically evaluated at the PCC point for the steady-state condition. If the OWPP does not fulfill these limits, the OWPP must be disconnected from the main grid with its associated consequences.

There is a vast number of references, e.g., [5]–[9] to cite some, that focus on OWPP stability studies. In these references, attention is paid on parallel resonances and controller aspects (e.g., bandwidth of current-control loops, feedforward terms, bandwidth of

The associate editor coordinating the review of this manuscript and approving it for publication was Siqi Bu.

measurement filters, etc.) but they do not assess if the OWPP system meets the harmonic limits imposed by the grid codes.

On the contrary, references [1], [10], [11] provide valuable contributions to the study of harmonics and stability in OWPPs. References [1] and [11] present the development of systematic methods for harmonic studies in wind power installations. In these references, the harmonic distortion of a WPP, with WTs operating with a typical Carrier-Based PWM (CB-PWM) modulation, is presented and compared with field measurements. Some open aspects that require further investigation are stated in these references and are taken as basis for this paper. These are:

- The evaluation of different modulation strategies.
- Studies regarding the feasibility of installing harmonic filters (passive-, active- and hybrid-filters) at different nodes along the OWPP.

The aim of this paper is to conduct harmonic studies in OWPPs and evaluate grid code compliance from the power quality perspective. The studies addressed in this paper serve as complementary analysis and contribution to open problems presented in previous paragraph. A general picture of the studies and contributions of this paper are presented next.

First, the harmonic evaluation is performed by considering that wind turbines operate, similar as in reference [1], with a typical CB-PWM modulation. This assessment is done at several operating points (not only at the rated condition) and at two levels of study, at the point of connection of the wind turbine (WTi-point) and at the point of connection of the OWPP or PCC-point.

Then, WT manufacturer solutions are proposed to improve the harmonic emission of the OWPP with the aim of reducing the possibility of installing harmonic filters at the offshore and/or onshore substation. The implementation of a particular solution of Selective Harmonic Elimination (SHE-PWM) modulation, especially designed to suit with the features of the scenario under study, is presented together with complementary solutions to further improve the harmonic emission of the OWPP.

In order to conduct the previous studies, a proper modeling approach must be performed. In this sense, the main power components of an AC OWPP are modeled to represent harmonics up to 5 kHz (frequency range of study).

For that objective, this paper exploits the strengths and applicability of the WT harmonic model proposed in reference [12] to represent the harmonic emission of a real grid side converter (GSC). In this sense, it is possible to represent the magnitude and phase of harmonics that are injected by WTs, which mainly depend on the type of modulation strategy and control loops. It is important to remark that experimental results at WT level, provided in [12], are used in this paper to account for real data of the harmonic emission of WTs.

The modeling approach also accounts for the representation of the frequency-dependent behavior of transformers and submarine cables. This last component is represented by means of the FDPi model proposed in [13].

Furthermore, Jensen's wake effect model is implemented to estimate the mean wind speed at each WT according to the spatial distribution of the OWPP and wind conditions. This allows the evaluation of different operating points (i.e., active power generation scenarios) according to reality.

As the main contribution of this paper, the studies and the modeling approach presented here serve as a generic simulation tool for stakeholders within the wind power industry, to conduct harmonic studies and evaluate the grid code compliance of an OWPP from a power quality perspective and during the design stage of a wind power plant.

The paper is structured as follows. Section II presents the definition of an OWPP base scenario and the current harmonic limits according to the BDEW grid code. Section III covers the modeling approach that is applied to evaluate the fulfillment of grid codes in terms of harmonics and to represent the scenario under study.

Section IV addresses the harmonic evaluation of WTs operating with CB-PWM. In section V, WT manufacturer oriented solutions are proposed with the aim of improving the harmonic emission of the OWPP and the compliance of the grid code. Section VI presents some aspects regarding the robustness evaluation of the solutions proposed in the previous section when considering parameter uncertainties. Finally, section VII gives the conclusion.

II. DEFINITION OF AN OWPP BASE SCENARIO AND SPECIFICATION OF HARMONIC LIMITS

As the first step, it is required to specify a case study and the harmonic limits according to a specific grid code. These aspects are covered next.

A. DEFINITION OF OWPP BASE SCENARIO

The base scenario is defined taking into account information of a real OWPP. The real OWPP, taken as reference, is Alpha Ventus offshore wind farm [14]. The main reason for its selection among other OWPPs is that general information regarding voltage levels at different buses, wind farm layout, grounding scheme, and main electrical components are known.

It is important to emphasize that even though the OWPP base scenario is defined based on Alpha Ventus, it is not an exact reproduction. It is also worthy to point out that certain parameters, required for the modeling of the main power components have been assumed due to lack of information. The assumptions were made according to supporting references and datasheets of other power components.

Fig. 1 depicts the simplified single-line diagram of the OWPP base scenario. The OWPP base scenario has a total capacity of 60 MW. This amount of power is generated from twelve type-4 WTs.

The step up transformer installed inside the WTs, hereafter called wind turbine transformer (WTT), increases the converter voltage level from 3.3 kV to 30 kV, which is the voltage level of the collection network. The windings of the WTT are Dyg1 connected.

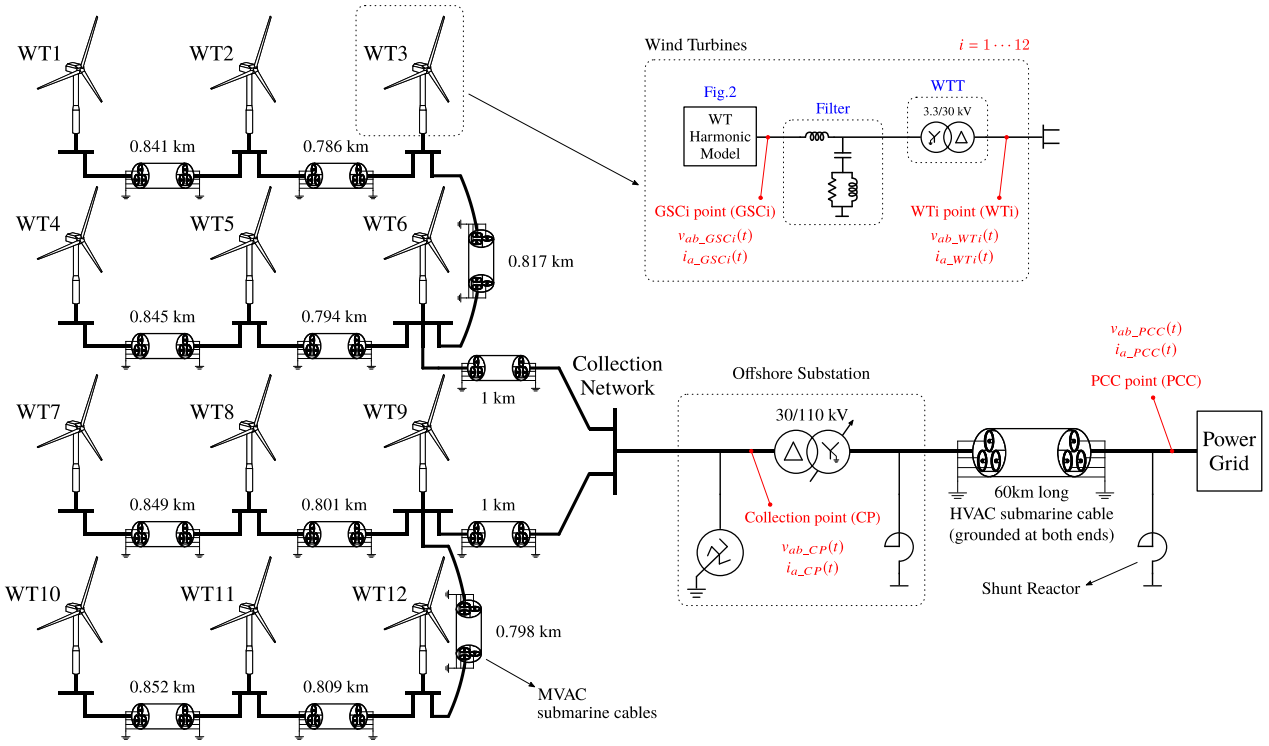

FIGURE 1. Simplified single-line diagram of the OWPP base scenario.

The WTs are clustered into groups of three forming a collection network with a rectangular shape. Information about the wind farm layout and the distance of each submarine cable of the collection network is shown in Fig. 1. Redundant connections are not implemented for this base scenario.

The collection network then links all the WTs to an offshore platform.

The offshore platform has a step-up transformer and a grounding transformer. This step-up transformer, here after called offshore substation transformer (OST), increases the voltage of the collection network to 110 kV, which is the voltage level of the transmission system. The OST has a rated power of 75 MVA and the windings are Ygd1 connected. The grounding transformer provides a neutral in the three-phase, three-wire system of the collection network.

The link between the offshore substation to shore is done by a single three-core submarine cable of 60 km long. The screens and armour of the submarine cables of the collection network and transmission system are grounded at both ends as depicted in Fig. 1.

Shunt reactors are installed at both ends of the transmission system. The purpose of those reactors is the management of the reactive power through the 60 km long submarine cable [15]. The energy transmission of the OWPP is improved since these shunt reactors reduce the required rated current of the cable and the active power losses.

Finally, the OWPP is connected to the main power grid of 110 kV.

B. SPECIFICATION OF CURRENT-HARMONIC LIMITS ACCORDING TO THE BDEW GRID CODE

The BDEW technical guideline [16] defines the maximum current injection limit of individual harmonic components, up to 9 kHz, according to Table 1.

According to the complementary rules [17] done to the original technical guideline, the integer harmonics and high frequency harmonics are calculated (since January 2013) as,

$$I_{vAzul} = i_{vzul} \cdot S_{kV} \cdot \sqrt{\frac{S_A}{S_{Gesamt}}} \tag{1}$$

In addition, interharmonics are computed as,

$$I_{\mu Azul} = i_{\mu zul} \cdot S_{kV} \tag{2}$$

Being,

S_A: Apparent connection power of the generating plant to be assessed.

S_{Gesamt}: Total connectable or planned feed-in power at the junction point under consideration.

S_{kV}: Short-circuit power at the junction point under consideration.

Furthermore, reference [17] defines some additional rules. The approval for certification is achieved if no more than six calculated values exceed the admissible limits defined in Table 2. Even-numbered harmonic currents are exempted from the calculation.

TABLE 1. BDEW harmonic current injection limits related to the network short-circuit power. Source [16].

Harmonic (v,μ)	Admissible i_{v,μ_zul} in A/MVA
	30 kV network
5	0.019
7	0.027
11	0.017
13	0.013
17	0.007
19	0.006
23	0.004
25	0.003
$25 < v < 40$ Odd-numbered	$0.003 \cdot 25/v$
Even-numbered	$0.02/v$
$\mu < 40$	$0.02/v$
$\mu, v > 40$ Integer and non-integer within a range of 200 Hz	$0.06/v$

TABLE 2. Admissible limit values for certification approval [17].

Harmonic order	Admissible limits
$6n \pm 1$ with $n = 1 \cdots 4$	< 200% BDEW limit
Remaining integer harmonics	< 400% BDEW limit
Interharmonics	< BDEW limit

III. MODELING FOR HARMONIC EVALUATION OF AN OWPP

Once the OWPP scenario and the current-harmonic limits are specified, it is important to disclose the modeling approach in order to perform the harmonic evaluation of the case study.

To account for an appropriate harmonic assessment of an OWPP, it is required to consider three important factors in the modeling [18]. First, an accurate representation of the harmonics injected by the wind turbines, i.e., including magnitude and phase of harmonics. Second, the frequency-dependent characteristic of installed passive components, e.g., submarine cables and transformers. The third factor to consider is the evaluation of different operating points (i.e., active- and reactive-power generation) for each wind turbine. These operating points depend on wind conditions, wind farm layout, and requirements given by the grid operator. These three aspects are covered next.

A. WIND TURBINE HARMONIC MODEL

The wind turbines of the OWPP scenario are modeled according to the schematic depicted in Fig. 2. Since the aim of this paper is to study the applicability of the model and not a deeper study of it, the reader is suggested to review reference [12] for more details.

Fig. 2 shows the schematic diagram of the WT harmonic model based on the WECC type-4 WT generic model. The main idea of this model is to emulate the grid side converter (GSC) and its control. This is done by implementing simplified structures that represent the dynamic behavior of the WTs (without a high computational burden) and the implementation of a voltage source containing both, the fundamental component and the harmonics emitted by the GSC converter.

The voltage commands are in d-q reference frame. The voltage is limited once the output voltage module is computed in order to not exceed the maximum voltage that can be generated by the implemented modulation strategy. This limited voltage is used to estimate the amplitude modulation index m_a, which is required by the harmonic synthesis block.

The time response of the converter output voltage can be synthesized using the Fourier series expansion. Assuming a null mean value and considering a finite number of harmonics, the converter output voltage for each phase with respect to the DC-link bus midpoint can be approximated by equations (3), (4) and (5).

Where ω_1 is the angular frequency of the fundamental component, $A_{n,m}$ is the magnitude of the n^{th} harmonic for the m^{th} amplitude modulation index, and $\theta_{n,m}$ corresponds to the phase of the n^{th} harmonic for the m^{th} amplitude modulation index. Furthermore, δ is the phase shift between the converter output voltage and grid voltage in order to control the power flow.

Therefore, both modulation strategies presented in this paper (CB-PWM and SHE-PWM) are implemented by means of a table of harmonics and a computation algorithm block shown in Fig. 2. This table has values of frequency, magnitude, and phase for different m_a values as depicted in Table 3 for illustrative purpose. The table of harmonics takes into account 99 member of Fourier series. This means the representation of harmonics up to a frequency of 5 kHz.

$$v_{a0\_GSC}(t) \approx m_a \frac{V_{Bus}}{2} \sin(\omega_1 t + \delta) + \sum_{n=2}^{N} \left\{ A_{n,m} \sin\left[n(\omega_1 t + \delta) + \theta_{n,m} \right] \right\} \tag{3}$$

$$v_{b0\_GSC}(t) \approx m_a \frac{V_{Bus}}{2} \sin\left(\omega_1 t - \frac{2\pi}{3} + \delta\right) + \sum_{n=2}^{N} \left\{ A_{n,m} \sin\left[n\left(\omega_1 t - \frac{2\pi}{3} + \delta\right) + \theta_{n,m} \right] \right\} \tag{4}$$

$$v_{c0\_GSC}(t) \approx m_a \frac{V_{Bus}}{2} \sin\left(\omega_1 t + \frac{2\pi}{3} + \delta\right) + \sum_{n=2}^{N} \left\{ A_{n,m} \sin\left[n\left(\omega_1 t + \frac{2\pi}{3} + \delta\right) + \theta_{n,m} \right] \right\} \tag{5}$$

As shown in Fig. 2, the model sets the fundamental component of the voltage from the voltage setpoints, which are defined by the GSC control block. On the contrary, for harmonics greater than the fundamental component, the model searches the required m_a value in the table and synthesizes the remaining $N-1$ spectral components. When the required m_a value is not defined in the table, the $A_{n,m}$ and $\theta_{n,m}$

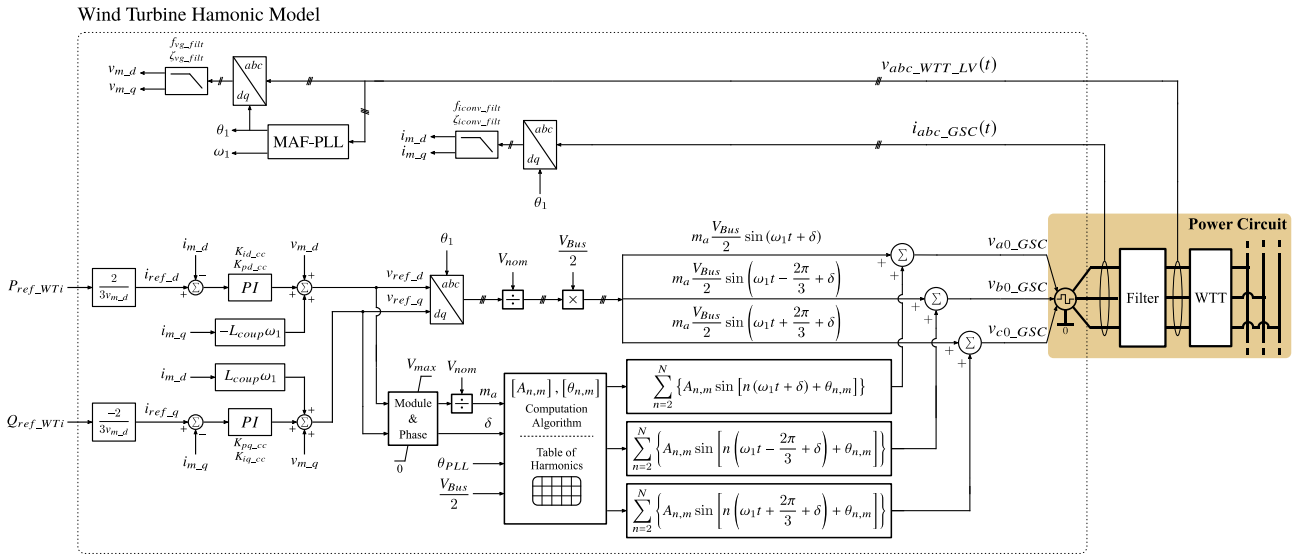

FIGURE 2. Wind turbine harmonic model – schematic diagram of the WT harmonic model based on the WECC type-4 generic model. Source [12].

TABLE 3. Table of harmonic content for a specific case of SHE-PWM, phase-angles are related to the angle of the fundamental component. Source [12].

Harmonics		Amplitude modulation index (m_a)				
		…	0.838	0.878	0.918	…
5th	$A_{5,m}$	…	0	0	0	…
	$\theta_{5,m}$	…	0º	0º	0º	…
7th	$A_{7,m}$	…	0	0	0	…
	$\theta_{7,m}$	…	0º	0º	0º	…
11th	$A_{11,m}$	…	0	0	0	…
	$\theta_{11,m}$	…	0º	0º	0º	…
13th	$A_{13,m}$	…	0	0	0	…
	$\theta_{13,m}$	…	0º	0º	0º	…
17th	$A_{17,m}$	…	0.074	0.108	0.12	…
	$\theta_{17,m}$	…	180º	180º	0º	…
19th	$A_{19,m}$	…	0.038	0.073	0.154	…
	$\theta_{19,m}$	…	180º	180º	180º	…
23th	$A_{23,m}$	…	0.08	0.071	0.036	…
	$\theta_{23,m}$	…	0º	0º	0º	…
25th	$A_{25,m}$	…	0.109	0.103	0.022	…
	$\theta_{25,m}$	…	0º	0º	0º	…
29th	$A_{29,m}$	…	0.119	0.046	0.006	…
	$\theta_{29,m}$	…	180º	180º	180º	…
⋮	⋮	⋰	⋮	⋮	⋮	⋱
99th	$A_{99,m}$	…	0.012	0.058	0.038	…
	$\theta_{99,m}$	…	0º	0º	0º	…

computation algorithm takes the upper and lower value that is defined in the table and performs a linear interpolation of the magnitude of the harmonic. For the phase, the nearest value is chosen. The inherent error, as a result of these simplifications, is reduced by considering a greater number of m_a values.

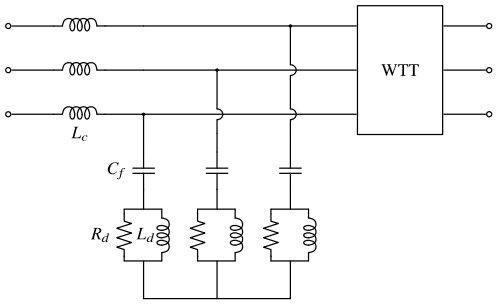

FIGURE 3. GSC connection filter schematic.

It is worth to mention that this way of modeling is validated in reference [12] with real measurements on a downscaled version of the INGECON WIND MV100 converter.

Once the WT harmonic model is briefly described, it is important to provide information regarding the features of the wind turbines that are depicted in Fig. 1. Table 4 gives the parameters of the WT harmonic model in order to represent the WTs of the OWPP base scenario.

Finally, Fig. 3 depicts the schematic of the filter that is used at the output of the converter. It is an LCL filter with a damping circuit formed by resistor R_d and inductor L_d. This type of damping circuit reduces the losses in the damping resistor, because the inductor provides a new path without losses to the fundamental current-component of the filter.

Table 5 gives the parameters of the GSC connection filter. This filter is designed according to the methodology presented in reference [19] in which it is considered a type-4 WT, the harmonic spectrum of a CB-PWM modulation (presented in section IV), and the BDEW grid code in terms of harmonics already presented in section II.

TABLE 4. Parameters of the wind turbine harmonic model.

Parameter	Value
Wind Turbines	
Active power (P_{WT})	5 MW
Number of WTs (N_{WTs})	12
Grid Side Converter	
Topology	3L-NPC
Rated output voltage (U_{GSC})	3.3 kV
DC-link bus voltage (V_{Bus})	5700 V
Modulation strategy	CB-PWM
Switching frequency (f_{sw})	1150 Hz
Current Control Loop	
Proportional gain d-axis (K_{pd_cc})	0.1426
Integral gain d-axis (K_{id_cc})	4.8652
Proportional gain d-axis (K_{pq_cc})	0.1426
Integral gain d-axis (K_{iq_cc})	4.8652
Coupling inductive term (L_{coup})	675 µH
MAF-PLL	
Proportional gain (K_{p_pll})	20
Integral gain (K_{i_pll})	70
Maximum rate of change of frequency (f_{max_rate})	12 Hz/s
Filter cut-off frequency (f_{fmeas_filt})	25 Hz
GSC Current Measurement Filter	
Type	Second-order LPF
Natural frequency (f_{iconv_filt})	200 Hz
Damping factor (ζ_{iconv_filt})	1
Grid Voltage Measurement Filter	
Type	Second-order LPF
Natural frequency (f_{vg_filt})	200 Hz
Damping factor (ζ_{vg_filt})	1

TABLE 5. Parameters of the GSC connection filter.

Parameter	Value
Converter side inductance (L_c)	675 µH
Filter capacitance (C_f)	270 µF
Damping circuit resistance (R_d)	0.52 Ω
Damping circuit inductance (L_d)	190 µH

The value of the grid side inductor is not given since this value is defined by the short-circuit inductance of the WT transformer which is presented later on.

B. TRANSFORMER MODEL

The power transformers of the OWPP scenario are modeled considering the saturable transformer component (STC) model and extending its representation in frequency up to 5 kHz. Fig. 4 shows the frequency-dependent STC model of a two-winding three-legged stacked core transformer.

The model includes the following:

- Frequency-dependent short-circuit impedance.
- Linear core impedance.
- Zero-sequence impedance.

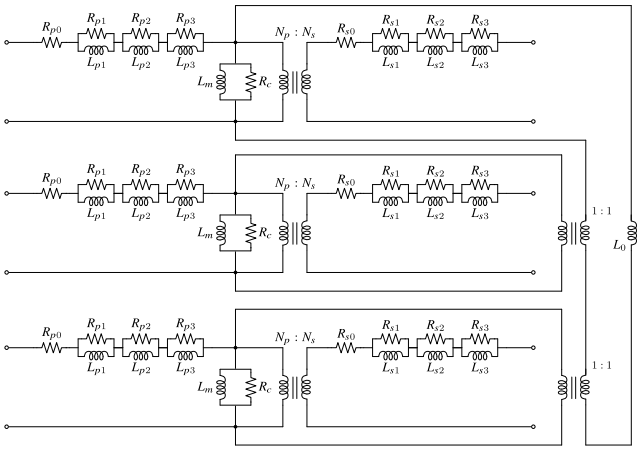

FIGURE 4. Frequency-dependent STC model for a two-winding three-legged stacked core transformer.

TABLE 6. Parameters of the wind turbine transformers (WTT).

Parameter	Value
Rated primary/secondary voltages (U_{HV}/U_{LV})	30/3.3 kV
Rated power (S_{WTT})	5 MVA
Short-circuit impedance (Z_{sc})	0.095 pu
X_{WTT}/R_{WTT} ratio ($\tan\theta_{sc}$)	11.26 pu
No load losses (at rated power)	0.002 pu
Magnetizing current (at rated power)	0.5%

TABLE 7. Parameters of the offshore substation transformer (OST).

Parameter	Value
Rated primary/secondary voltages (U_{HV}/U_{LV})	110/30 kV
Rated power (S_{OST})	75 MVA
Short-circuit impedance (Z_{sc})	0.095 pu
X_{OST}/R_{OST} ratio ($\tan\theta_{sc}$)	11.26 pu
No load losses (at rated power)	0.002 pu
Magnetizing current (at rated power)	0.5%

The parameters of the WTT and OST transformers are given in Table 6 and Table 7, respectively. ABB 2.35 MVA transformer data is considered and same per-unit values are used for parameterization due to lack of information.

To include the frequency-dependency of transformer winding resistance, the approach presented in reference [20] is used. The per-unit *R* and *L* parameters of the Foster equivalent network of order three are given in Table 8. This approach can be easily applied to any transformer in the range of 20-500 MVA by rescaling the given Foster circuit parameters by the 50 Hz winding resistance. For the case of the OST and WTT transformers, 100 MVA and 20 MVA transformer data is selected, respectively, since they are the closest information available to the real values.

Before continuing with the next power component, it is important to mention that if the values of stray C_{HG}, C_{LG},

TABLE 8. *R* and *L* parameters of the foster equivalent network of order three for transformer model.

Parameter	20 MVA	100 MVA	500 MVA
R_0/R_{50Hz}	0.85	0.85	0.85
R_1/R_{50Hz}	21.0768	33.4367	31.3912
R_2/R_{50Hz}	2205.3118	2176.8834	2080.7688
R_3/R_{50Hz}	2311.709	2483.8188	1723.2928
L_1/R_{50Hz}	$5.1203\cdot10^{-3}$	$6.2436\cdot10^{-3}$	$6.0033\cdot10^{-3}$
L_2/R_{50Hz}	$25.0870\cdot10^{-3}$	$28.0169\cdot10^{-3}$	$27.9849\cdot10^{-3}$
L_3/R_{50Hz}	$0.9745\cdot10^{-3}$	$1.0237\cdot10^{-3}$	$1.1650\cdot10^{-3}$
$R_{eq(50Hz)}/R_{50Hz}$	1.0002	1.0003	1.0001
$L_{eq(50Hz)}/R_{50Hz}$	$31.1519\cdot10^{-3}$	$35.2625\cdot10^{-3}$	$35.1312\cdot10^{-3}$

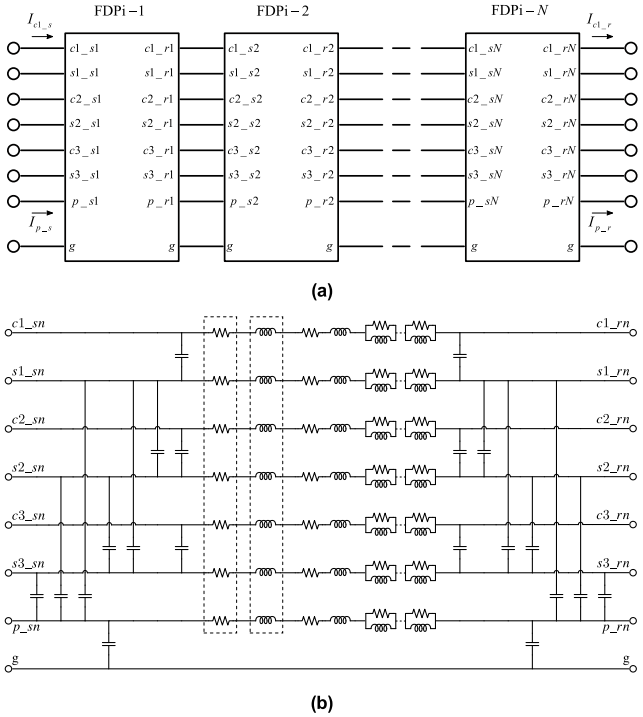

FIGURE 5. Frequency-Dependent Pi (FDPi) model of a three-core submarine cable. (a) Cascaded FDPi sections. (b) Detailed schematic of an FDPi section. Source [13].

and C_{HL} capacitances are known, they can be added to the model as well.

C. SUBMARINE CABLE MODEL

The submarine cables of the OWPP scenario are modeled considering the Frequency-Dependent Pi (FDPi) model proposed in reference [13]. Fig. 5 shows the electrical schematic of the FDPi model, which physically represents the seven conductors of the three-core submarine cables shown in Fig. 1.

As depicted in Fig. 5(a), the model consists of N-cascaded FDPi sections. Each FDPi section consists of a resistance- and inductance matrix computed at nominal frequency. The capacitive coupling between conductors is computed at nominal frequency as well.

The frequency-dependent behavior of the series impedance terms of each conductive layer is represented by means of a Foster equivalent network. The order of the FDPi model is given by the number of cascaded sections (N) together with the order of the Foster equivalent networks (M). The order of the model is chosen depending on the cable length, accuracy, and frequency range requirements. Being this last defined to represent frequencies up to 5 kHz.

The parameterization process of the MVAC submarine cables (collection network) and HVAC cable (transmission link) is performed according to the procedure presented in [13].

The parameters of the collection network cables are computed according to information of the Nexans 2XS2YRAA 18/30(36) kV three-core submarine cable [21]. Table 9 gives electrical and constructional data of this cable.

On the other hand, the parameters of the transmission link cable are computed according to information of ABB HVAC 110(130) kV three-core submarine cable [22]. Table 10 gives electrical and constructional data for this HVAC cable.

TABLE 9. Parameters of the MVAC collection network cables. Source [21].

Parameter		Value
Constructional data		
Nominal cross-sectional area of conductor		240 mm^2
Conductor copper round stranded diameter		18.6 mm
Insulation XLPE wall thickness		8 mm
Screen copper wires and counter helix cross-section		25 mm^2
Core sheath PE black	Wall thickness	2.5 mm
	Diameter	43 mm
Bedding wall thickness		2 mm
Armour steel wires round galvanized diameter		5 mm
Serving bitumen and lime wash wall thickness		4 mm
Outer diameter of the cable		114 mm
Electrical data		
Series resistance $(\hat{R})$		0.0886 Ω/km
Series inductance $(\hat{L})$		0.3351 mH/km
Shunt capacitance $(\hat{C})$		0.23 μF/km
Number of FDPi sections (N_{FDPi})		1

TABLE 10. Parameters of the HVAC transmission link cable. Source [22].

Parameter	Value
Constructional data	
Cross-section of conductor	240 mm^2
Diameter of conductor	18.1 mm
Insulation thickness	15 mm
Diameter over insulation	50.5 mm
Lead sheath thickness	2 mm
Outer diameter of the cable	157 mm
Electrical data	
Series resistance $(\hat{R})$	0.0847 Ω/km
Series inductance $(\hat{L})$	0.3927 mH/km
Shunt capacitance $(\hat{C})$	0.15 μF/km
Number of FDPi sections (N_{FDPi})	20

TABLE 11. Parameters of the shunt reactors.

Parameter	Value
Offshore substation shunt reactor	10 MVAr fixed shunt reactor
Onshore substation shunt reactor	11.7 MVAr fixed shunt reactor

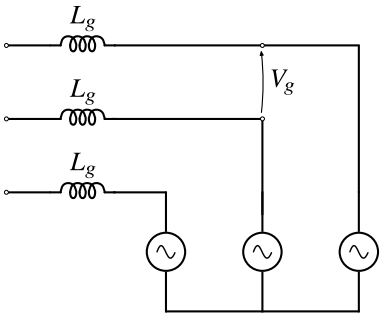

FIGURE 6. Power grid model. Source [15].

D. SHUNT REACTORS

As pointed out in section II.A, shunt reactors are installed at both ends of the transmission system to reduce the effect of the capacitance generated by the 60km long HVAC submarine cable and to work with a power factor close to one.

According to a report of the National Grid ESO [23], Alpha Ventus offshore substation has a 10 MVAr 110kV fixed shunt reactor supplied by Areva. This reactive value is considered for the studies presented in this paper.

For the case of the onshore substation, a fixed shunt reactor of 11.7 MVAr is considered. It is important to mention that variable compensators, e.g. Thyristor-Controlled Reactors (TCR) and Static Synchronous Compensators (STATCOMs), are only needed when there are very strict requirements at the PCC point of the OWPP, i.e. when it is required complete reactive power compensation. This case is only fulfilled for certain operating points evaluated in this paper. Further studies can be done in this direction to evaluate more scenarios.

Table 11 gives the values of the shunt reactors considered for the OWPP base scenario.

E. POWER GRID MODEL

The power grid is modeled as an ideal voltage source and a short-circuit impedance. The short-circuit impedance is considered an inductor as a simplification according to reference [15]. A grid with a short-circuit ratio (SCR) equal to 20 (strong grid) is considered for the OWPP base scenario and the studies carried out in sections IV and V. In section VI, the harmonic evaluation is tested for an SCR value of five, which represents a weak grid.

Fig. 6 shows the schematic of the power grid model and Table 12 provides its parameters.

It is important to note that the short-circuit impedance of the power grid model can be represented as a frequency-dependent network, instead of the simplified inductor, to account for capacitive- and inductive-behavior at different frequency ranges. In order to do so, information of the transmission system operator (TSO) is required to simulate a scenario as close as possible to reality.

TABLE 12. Parameters of the power grid.

Parameter	Value
Nominal voltage (U_N)	110 kV
Short-circuit ratio (SCR)	20
Nominal frequency (f_1)	50 Hz

F. WAKE EFFECT MODEL

Jensen's model is adequate in order to estimate the mean wind speed at each WT according to the spatial distribution of the OWPP and wind conditions (speed and direction). This allows to address the harmonic assessment according to reality at different operating points and not just for the rated one.

Jensen's model has been chosen due to the following features [24], [25]:

- Simply and widely used model.
- Low computational load.
- Accuracy is similar to more complex models.

According to Jensen's wake model, equation (6) describes the downstream wind speed of a single WT [26].

$$V_{wind,x} = V_{wind,0}\left[1 - \frac{1-\sqrt{1-C_T}}{\left(1+\frac{2k_{wdc}x}{D_{turbine}}\right)^2}\right] \tag{6}$$

Being,

$V_{wind,0}$: free stream wind.

$V_{wind,x}$: wind speed at distance x from the WT.

x: distance behind the turbine.

$D_{turbine}$: diameter of the turbine rotor.

C_T: thrust coefficient.

k_{wdc}: wake decay constant.

In an OWPP, the multiple wake effect among wind turbines should be taken into account. This can be done by empirical methods [27] such as sum of squares of velocity deficits, energy balance, geometric sum, and linear superposition.

The sum of squares of velocity deficits is chosen according to Katic recommendations [28]. In this sense, the wind speed at WT_i, which is shadowed by the wake of wind turbines WT_j upstream, is given by equation (7) according to reference [27].

$$V_{wind,WT_i} = V_{wind,0}\underbrace{\left[1 - \sqrt{\sum_{j=1}^{N_{WTs,up}} \beta_{WT_{ij}}\left(1-\frac{V_{wind,WT_{ij}}}{V_{wind,0}}\right)^2}\right]}_{k_{WT_i}} \tag{7}$$

Being,

V_{wind,WT_i}: wind speed at WT_i.

$V_{wind,WT_{ij}}$: wind speed at WT_i due to the incidence of the wake of WT_j.

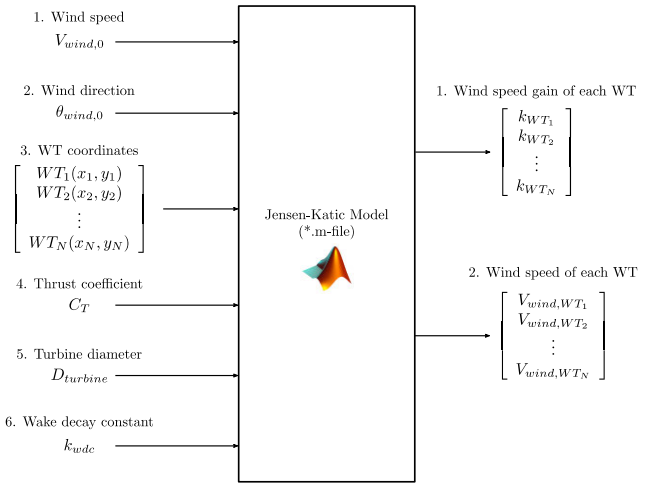

FIGURE 7. Wake effect tool schematic.

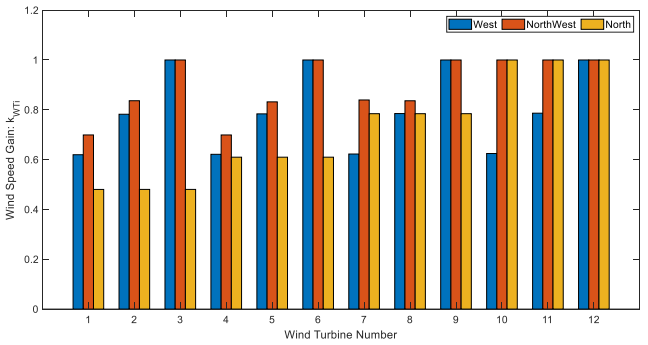

FIGURE 8. Wind speed gains of each WT for three different wind directions: west, northwest and north.

$N_{WTs,up}$: wind speed at WT_i.

$\beta_{WT_{ij}}$: ratio of the shadowed area by the wake in relation to the total rotor area A_{WT_i}.

Jensen's model has been implemented in a *.m-file in Matlab®. This script is added to the Simulink®-based model of the OWPP, thus considering WT wake effect in power system simulations. Fig. 7 depicts the input- and output variables required by the Matlab® script.

Table 13 gives the input parameters required by the tool. The turbine diameter corresponds to the value of the Multibrid M5000 wind turbine from AREVA manufacturer [29]. The values for the wake decay constant and thrust coefficient are assumed according to recommendations presented in [24].

Wind conditions are defined according to the wind rose presented in references [30], [31]. Three wind directions are considered for the studies in this paper. However, it is important to mention that other wind directions can be evaluated as well. The three wind directions are west, northwest, and north.

The wind speed gains k_{WTi}, for the twelve WTs and for the aforementioned wind conditions, are depicted in Fig. 8.

The power curve is used to compute the active power reference of each WT as depicted in Fig. 9. Note that this is a simplified model, in reality, the WTs implement a Maximum Power Point Tracking (MPPT) strategy.

TABLE 13. Input parameters of the wake effect tool.

Parameter	Value
Turbine diameter ($D_{turbine}$)	116 m
Thrust coefficient (C_T)	0.75
Wake decay constant (k_{wdc})	0.038
WT coordinates	Defined according to Fig. 1

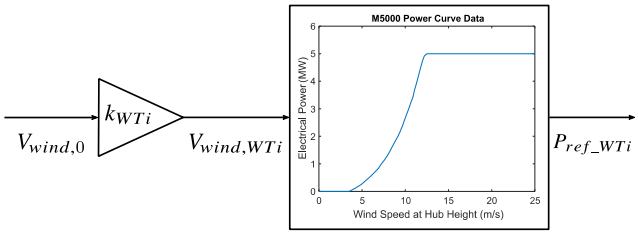

FIGURE 9. Computation of the active power reference of each WT.

Fig. 10 shows the active power references of each WT, i.e., the input values of P_{ref_WTi} variable of Fig. 2 model, for the wind directions and wind speeds that are evaluated in this paper. On the other hand, Fig. 11 depicts the estimated active power generation of the entire OWPP.

IV. HARMONIC EVALUATION FOR WTs OPERATING WITH CB-PWM MODULATION

This section carries out the harmonic evaluation for WTs operating with CB-PWM. For this modulation strategy, the harmonic assessment is performed at two points of the OWPP, WT point and PCC point (see Fig. 1), and for several operation conditions.

Fig. 12 shows the harmonic spectrum of a typical CB-PWM modulation. Fig. 12(a) depicts the harmonic spectrum of phase "a" with respect to the midpoint of the DC-link. On the other hand, Fig. 12(b) shows the line-to-line harmonic spectrum.

As noticed in Fig. 12(a), the frequency modulation index m_f is equal to 23. Since this value is not a multiple of three, each odd harmonic has positive-, negative- and zero-sequences. Additionally, the harmonic spectrums shown in this figure reveal the generation of low order harmonics (e.g. 3rd, 5th, 7th, 9th, etc.).

A. EVALUATION AT WT POINT

Fig. 13 shows the harmonic spectrum of the current-signal $i_{a\_WT1}(t)$ at rated condition. The figure also shows the current-harmonic limits imposed by the BDEW grid code at WT point. Table 14 gives a summary of the compliance of the grid code for different operating points considering several wind speeds and directions. For the evaluated cases, the wind turbine is not injecting reactive power to the grid.

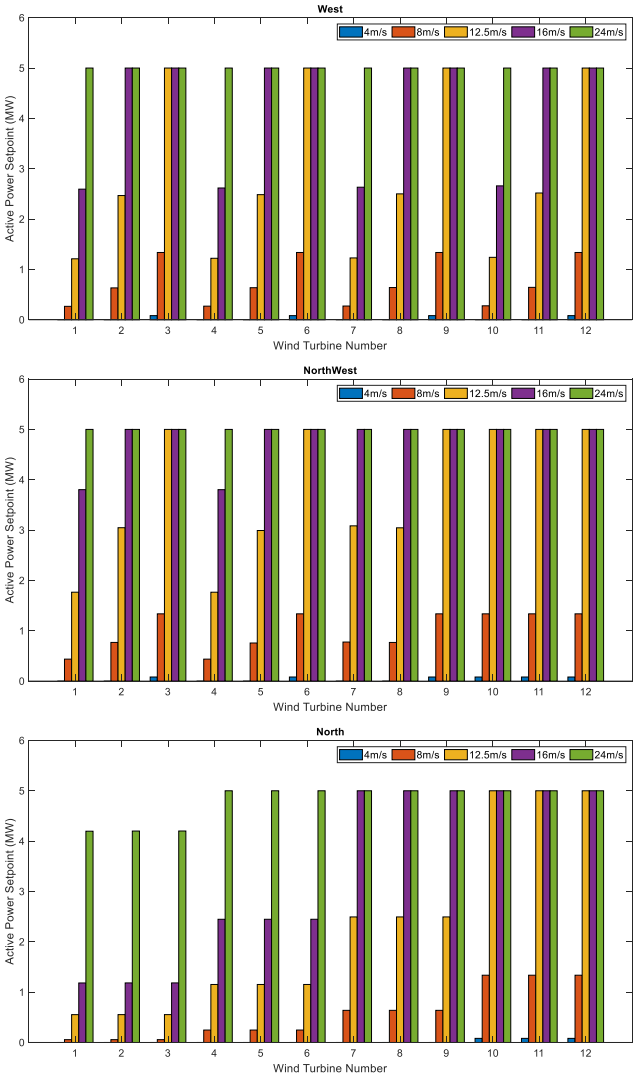

FIGURE 10. Estimated active power generation (P_{ref_WTi}) of each WT for the wind conditions evaluated in this article.

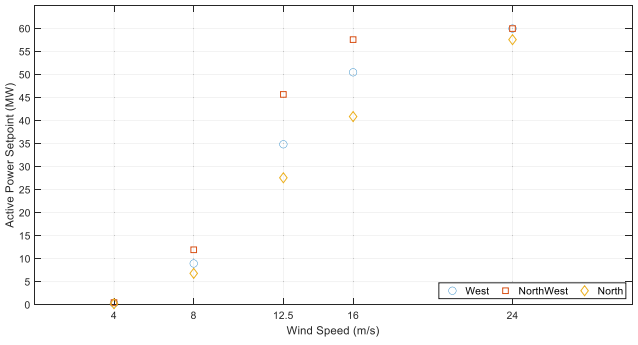

FIGURE 11. Estimated active power generation of the OWPP for the wind conditions evaluated in this article.

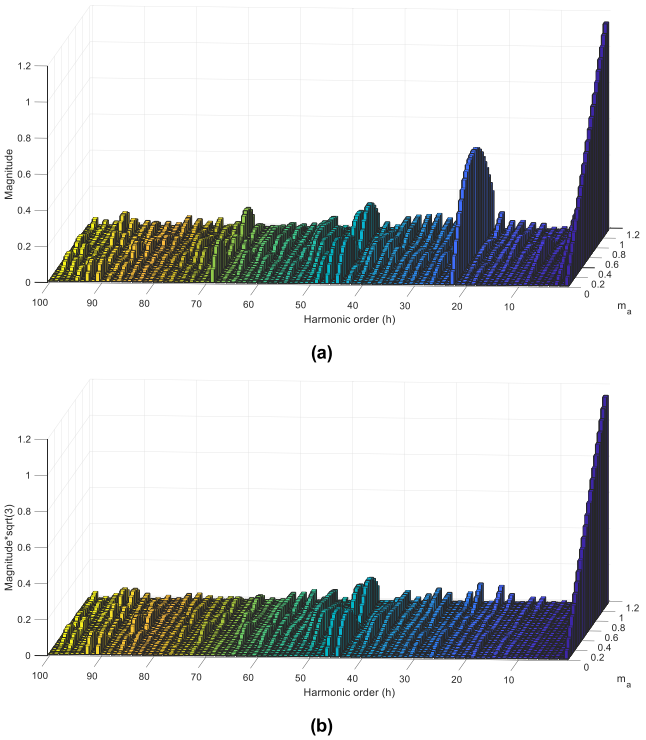

FIGURE 12. Harmonic spectrum of CB-PWM modulation as a function of the amplitude modulation index. (a) Phase "a" with respect to the midpoint "0" of the DC-link. (b) Line-to-line harmonic spectrum.

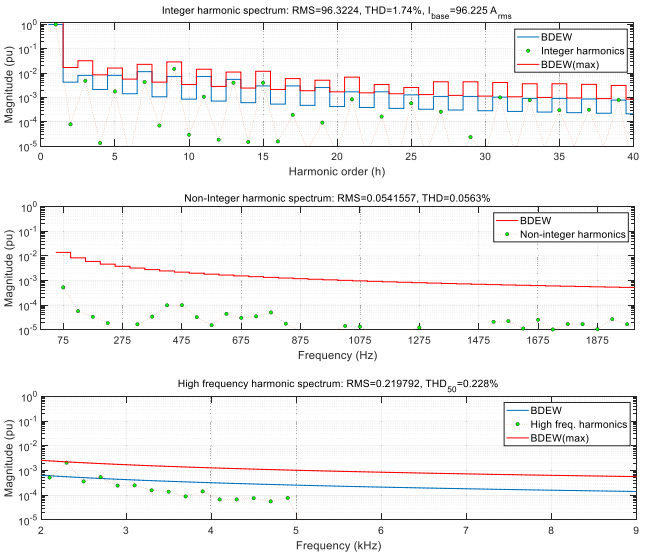

FIGURE 13. Harmonic spectrum of current signal $i_{a\_WT}(t)$ plotted against the BDEW harmonic current limits at WT point (SCR = 20). This scenario considers WTs operating at rated condition (wind direction = west, wind speed = 24 m/s) and CB-PWM modulation.

According to Fig. 13 and Table 14, the BDEW grid code is fulfilled for the evaluated operating points since there are no infringement of the technical rules pointed out in section II. It is important to point out that the compliance of the grid code at this level is mainly due to the proper design of the LCL filter to meet grid code requirements related to current-harmonics.

Even though the BDEW grid code is fulfilled, it is of major significance to be aware of low order harmonics and especially harmonics of order 45th and 47th since exceeding

TABLE 14. Compliance of the BDEW grid code at WT point for CB-PWM and for different operating points.

WT Power (% Pn)	BDEW Comp.	Harmonic (h)	Infringement of BDEW limits for harmonics of order		
			$6n \pm 1$ with $n = 1 \cdots 4$	Others	Inter-harmonic
		>BDEW limit	>200% BDEW limit	>400% BDEW limit	>BDEW limit
>95%	Yes	9,15,45,47	–	–	–
80%	Yes	9,15,45,47	–	–	–
60%	Yes	9,15,45,47	–	–	–
40%	Yes	9,15,45,47	–	–	–
20%	Yes	9,15,45,47	–	–	–

TABLE 15. Total harmonic distortion at WT point for CB-PWM and for different operating points.

WT Power (% Pn)	Low Frequency		Interharmonics		High Frequency	
	RMS (A)	THDi (%)	RMS (A)	THDi (%)	RMS (A)	THDi (%)
>95%	96.32	1.74	0.0541	0.0563	0.2197	0.228
80%	76.85	1.74	0.0381	0.0397	0.2199	0.229
60%	57.53	1.73	0.0356	0.0371	0.2201	0.229
40%	38.29	1.71	0.0398	0.0414	0.2203	0.229
20%	19.11	1.70	0.0310	0.0322	0.2202	0.229

the BDEW(max) curve will provoke the non-fulfillment of the grid code.

Table 15 gives the total harmonic distortion (THDi) values of the current-signal $i_{a\_WT}(t)$ for WTs operating with CB-PWM and for different operating points. The THDi values are computed for the three harmonic subgroups specified by the BDEW grid code.

By looking at the results of Table 15, it can be noticed that similar THDi values are obtained when comparing the same harmonic subgroup for the evaluated operating points.

B. EVALUATION AT PCC POINT

Once the harmonic spectrum of the CB-PWM modulation and the compliance of the grid code at WT point are presented, it is important to identify the possible risk of harmonic amplification at the PCC point. This identification is performed by means of two steps.

- First, by analyzing the transfer functions that relate the current at the PCC point of the OWPP with respect to the GSC voltage of each WT. In this way, it is possible to determine whether the harmonics are added in phase or not.
- Second, by identifying the harmonics that might not fulfill the grid code. This is done by taking into account both, the injected harmonics and the level of attenuation that sees each harmonic component.

For the first step, Fig. 14 shows the Bode plots of transfer functions $I^{+}_{a\_PCC}(s)/V^{+}_{ab\_GSCi}(s)$ of the OWPP base scenario. As shown in this figure, the Bode plots of these transfer

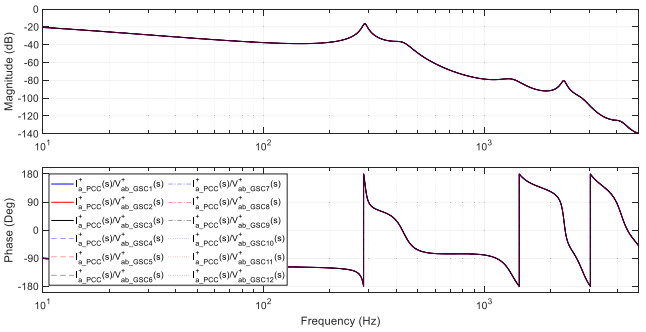

FIGURE 14. Bode plot of transfer functions $I^{+}_{a\_PCC}(s)/V^{+}_{ab\_GSCi}(s)$ of the OWPP base scenario.

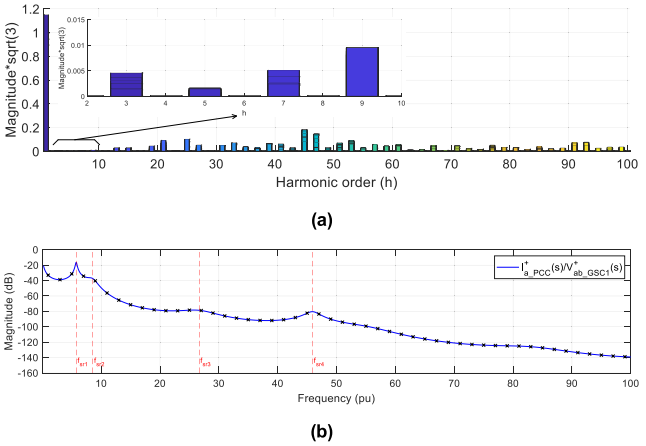

FIGURE 15. Risk of amplification of harmonics for GSCs using CB-PWM modulation. (a) CB-PWM line-to-line spectrum with different m_a values stacked. (b) Bode plot of transfer function $I^{+}_{a\_PCC}(s)/V^{+}_{ab\_GSC1}(s)$.

functions are almost equal for the frequency range of study. For higher frequencies, differences in magnitude and phase are increased.

An important aspect that can be inferred from Fig. 14 is that the electrical infrastructure of the OWPP does not cause a different phase shift (for frequencies up to 5 kHz) among the harmonics injected by the GSCs. In this sense, if the GSCs work at the same (or almost the same) operating point, the magnitude of harmonics of the same order will be increased at the PCC point because these harmonics are added in phase. Additional increase, or lower attenuation level depending on the case, can be obtained if a resonance is near a specific harmonic.

Regarding the second step, Fig. 15(a) shows the CB-PWM line-to-line spectrum of the voltage-signal $v_{ab\_GSCi}(t)$ in a 2D-plane for different m_a values. Fig. 15(b) depicts the Bode plot of transfer function $I^{+}_{a\_PCC}(s)/V^{+}_{ab\_GSC1}(s)$, which is also valid for the negative-sequence $I^{-}_{a\_PCC}(s)/V^{-}_{ab\_GSC1}(s)$. This figure highlights the first four series resonances with a red dashed line and the value taken for each harmonic with a black cross marker.

Table 16 gives the damped frequency, damping factor and dominant state variables that create these resonances. This

TABLE 16. Dominant state variables and power components that create the first four series resonances of the OWPP base scenario.

Series Resonance	Frequency	Damping Factor	Dominant State Variable (Component)
f_{sr1}	287.89 Hz	0.0236	vC.tc (Tx cable) iLg (Grid)
f_{sr2}	429.11 Hz	0.0925	vCf.wti (GSC filter) iLc.wti (GSC filter) iLwtt.wti (WTT) iLost (OST) iLg (Grid)
f_{sr3}	1334.46 Hz	0.1084	vC.tc (Tx cable) iL.tc (Tx cable) iLg (Grid)
f_{sr4}	2296.84 Hz	0.0245	vC.cc (Collection cables) iLost (OST) iLwtt.wti (WTTs)

information is obtained by means of computing the participation factors of the system [32], [33].

The first series resonance f_{sr1}, whose frequency is near 5th and 7th order harmonics, is mainly created by the capacitance of the transmission cable and the equivalent inductance of the grid.

Resonance f_{sr2}, which is near harmonic of order 9, is greatly created by the GSC connection filter. On the other hand, resonance f_{sr3} is mainly created by the transmission cable (its second series resonance).

Finally, resonance f_{sr4} is created by the combination of the capacitance of the collection network cables and the short-circuit inductance of the OST and WTTs.

Analyzing Fig. 15 as a whole, it can be seen that harmonics of order 5th and 7th are the most affected despite the fact that their magnitudes are very low and that resonance f_{sr1} does not match perfectly with them. The level of attenuation is relatively low around -30dB.

As pointed out, if the GSCs work at the same operating point, the harmonics of the same order are added because they are in phase. Hence, their magnitude is increased by this characteristic at the PCC point. Consequently, these conditions affect the distortion of voltage- and current-signals at the PCC point, which might endanger the compliance of the grid codes. In this sense, the aforementioned harmonics might be considered an issue in terms of level of distortion and compliance of the grid codes.

For harmonics of order 25th and 27th, it can be seen that even their magnitudes are higher than harmonics of low order, the attenuation around resonance f_{sr3} is considerably higher than the previous case. Therefore, it seems that these harmonics might not be an issue.

Finally, the situation changes for harmonics of order 45th and 47th. The magnitude of these harmonics can be much higher when comparing to previous harmonics. Furthermore, the attenuation level around resonance f_{sr4} is very similar to resonance f_{sr3}. In this sense, it seems that these harmonics might endanger the fulfillment of the grid code.

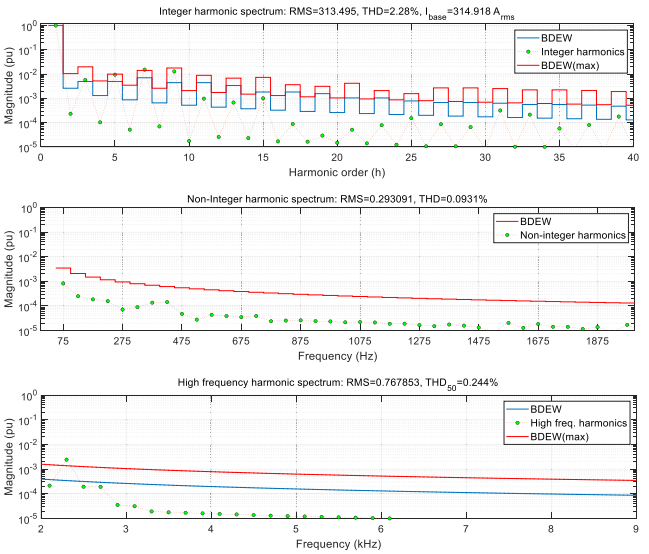

FIGURE 16. Harmonic spectrum of current signal $i_{a\_PCC}(t)$ plotted against the BDEW harmonic current limits at PCC point (SCR = 20). This scenario considers WTs operating at rated condition (wind direction = west, wind speed = 24 m/s), $V_{bus} = 5700\ V$, $m_a \approx 0.91$ and CB-PWM modulation.

These statements are corroborated next by means of the Simulink®-based model addressed in section III and different wind conditions, i.e., different speeds and directions.

Fig. 16 shows the harmonic spectrum of the current-signal $i_{a\_PCC}(t)$ at rated condition. The figure also shows the current-harmonic limits imposed by the BDEW grid code at PCC point.

As noticed from this figure, the grid code is not fulfilled for the evaluated operating point due to the infringement of harmonics of order 7th, 45th and 47th (these last two harmonics represent the calculated harmonic of order 46th according to the computation guidelines given by [16]).

Table 17 gives a summary of the fulfillment of the grid code for different operating points. As can be seen, the BDEW grid code is not fulfilled for these evaluated conditions since the harmonics, stated previously, exceed the maximum limits.

Table 18 gives the total harmonic distortion (THDi) values of the current-signal $i_{a\_PCC}(t)$ for WTs operating with CB-PWM and for different operating points. The THDi values are normalized with respect to the base value at the PCC point.

As inferred from the data presented in Table 18, the THDi values of low- and high-frequency harmonics remain about the same as a function of the generated active power, around 2% for low frequency subgroup and around 0.24% for high frequency subgroup. On the other hand, the THDi values of interharmonic subgroup present an increase while increasing the produced active power.

Finally and due to the reasons stated in this section, it can be concluded that this modulation strategy (CB-PWM) is not suitable to be used for this OWPP scenario mainly due to the infringement of the grid code in terms of harmonics.

TABLE 17. Compliance of the BDEW grid code at PCC point for CB-PWM and for different operating points.

Wind Condition		BDEW Comp.	Harmonic (h)	Infringement of BDEW limits for harmonics of order:		
				$6n \pm 1$ with $n = 1 \cdots 4$	Others	Inter-harmonic
Dir.	m/s		>BDEW limit	>200% BDEW limit	>400% BDEW limit	>BDEW limit
W	24	No	3, 5, 7, 9, 45, 47	7	45, 47	–
	16	No	3, 5, 7, 9, 45, 47	7	45, 47	–
	12.5	No	3, 5, 7, 9, 45, 47	7	45, 47	–
	8	No	3, 5, 7, 9, 45, 47	7	45, 47	–
NW	24	No	3, 5, 7, 9, 45, 47	7	45, 47	–
	16	No	3, 5, 7, 9, 45, 47	7	45, 47	–
	12.5	No	3, 5, 7, 9, 45, 47	7	45, 47	–
	8	No	3, 5, 7, 9, 45, 47	7	45, 47	–
N	24	No	3, 5, 7, 9, 45, 47	7	45, 47	–
	16	No	3, 5, 7, 9, 45, 47	7	45, 47	–
	12.5	No	3, 5, 7, 9, 45, 47	7	45, 47	–
	8	No	3, 5, 7, 9, 45, 47	7	45, 47	–

TABLE 18. Total harmonic distortion at OWPP level for CB-PWM and for different operating points.

Wind Condition		Low Frequency		Interharmonics		High Frequency	
Dir.	Speed (m/s)	RMS (A)	THDi (%)	RMS (A)	THDi (%)	RMS (A)	THDi (%)
W	24	313.49	2.28	0.293	0.0931	0.7678	0.244
	16	264.96	2.15	0.248	0.0791	0.7666	0.243
	12.5	188.14	2.03	0.179	0.0571	0.7652	0.243
	8	83.73	2.25	0.115	0.0368	0.7666	0.243
NW	24	313.49	2.28	0.293	0.0931	0.7678	0.244
	16	301.13	2.26	0.282	0.0896	0.7676	0.244
	12.5	240.90	2.11	0.226	0.0721	0.7662	0.243
	8	92.64	2.26	0.104	0.0332	0.7668	0.244
N	24	301.10	2.27	0.282	0.0896	0.7677	0.244
	16	216.83	1.99	0.204	0.065	0.7649	0.243
	12.5	153.70	1.98	0.146	0.0467	0.7644	0.243
	8	78.47	2.24	0.131	0.0418	0.7664	0.243

V. WT ORIENTED SOLUTIONS TO IMPROVE THE HARMONIC EMISSION OF THE OWPP

Many mitigation techniques have been proposed and implemented in power systems, e.g. OWPPs, to maintain harmonic distortion within recommended levels. These are [34], [35]:

- Harmonic cancellation or mitigation by means of transformer connections. Phase shifting of harmonics is achieved by considering different winding connections (vector groups) or special transformers. For example:
  - Transformers with delta connections to trap and prevent zero-sequence harmonics from entering a specific zone of a power system.
  - Transformers with zigzag connections for cancellation of low order harmonics (e.g., harmonics of order 5 and 7) and compensation of load imbalances.
- Harmonic filters (passive-, active- and hybrid-filters) and power devices, such as Active Power Line Conditioners (APLCs) and Unified Power Quality Conditioners (UPQCs), placed at specific nodes along the OWPP (e.g. near the source of harmonics, at the PCC point or other problematic point in which the reliability of the entire system is not ensure).
- Implementation of different modulation strategies.
- Others.

From previous mitigation techniques, WT manufacturer oriented solutions are studied with the aim of improving the harmonic emission of the OWPP. According to the results presented in previous section, a modulation strategy that does not inject low-order harmonics is more suited to be used for the scenario under study. In this sense, the implementation of a particular solution of SHE-PWM modulation is studied together with complementary solutions to further improve the harmonic emission of the OWPP.

A. HARMONIC EVALUATION FOR WTs OPERATING WITH SHE-PWM MODULATION

SHE-PWM is the most common among all optimal PWM techniques [36]. In this technique, the exact instant of the commutations within a fundamental period is calculated so that the fundamental frequency is regulated to a certain amplitude while (m-1) harmonics, typically low-frequency harmonics, are also eliminated from the output voltage spectrum.

The main advantages of SHE-PWM lie in the tight control of the harmonic spectrum resulting in the elimination of low-order harmonics, reduction of the switching frequency, and relatively simple implementation based on pre-calculated switching angles and look-up tables.

Fig. 17 shows the harmonic spectrum of the particular solution of SHE-PWM modulation that is implemented with the aim of fulfilling the BDEW grid code and reducing the harmonic emission of the OWPP base scenario presented in section II.

The modulation depicted in Fig. 17 does not inject harmonics of order 5^{th}, 7^{th}, 11^{th}, and 13^{th}. The first non-eliminated harmonic that appears in the current is the harmonic of order 17^{th}. In contrast to the CB-PWM modulation shown in Fig. 12, each harmonic has only one sequence. The harmonics follow the sequence order of a square wave as presented in Table 19.

Once the harmonic spectrum of the particular solution of SHE-PWM is presented, it is important to identify the possible risk of harmonic amplification. This identification is performed by means of analyzing Fig. 18.

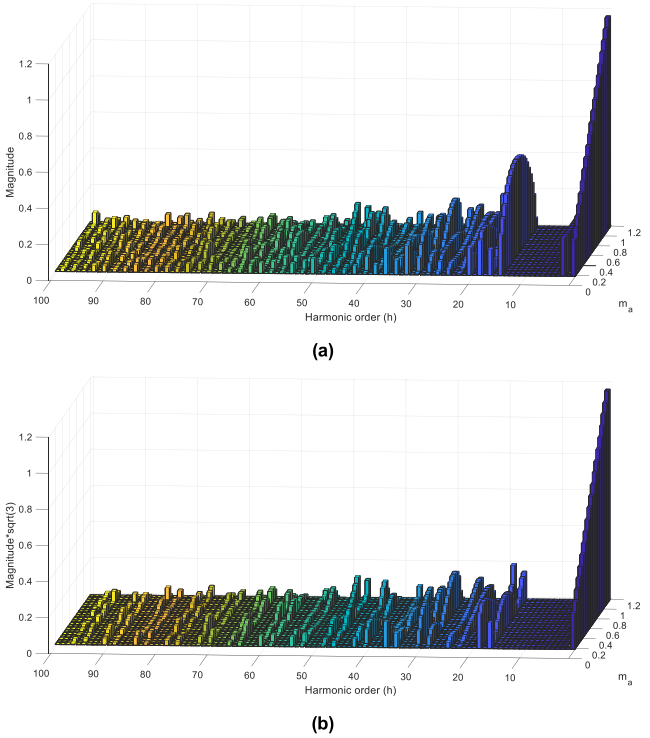

FIGURE 17. Harmonic spectrum of SHE-PWM modulation as a function of the amplitude modulation index. (a) Phase "a" with respect to the midpoint "0" of the DC-link. (b) Line-to-line harmonic spectrum.

TABLE 19. Sequence order of a square wave and the particular solution of SHE-PWM proposed in Fig. 17.

Harmonic	1	3	5	7	9	11	13	15	17	19	…
Sequence	+	0	-	+	0	-	+	0	-	+	…

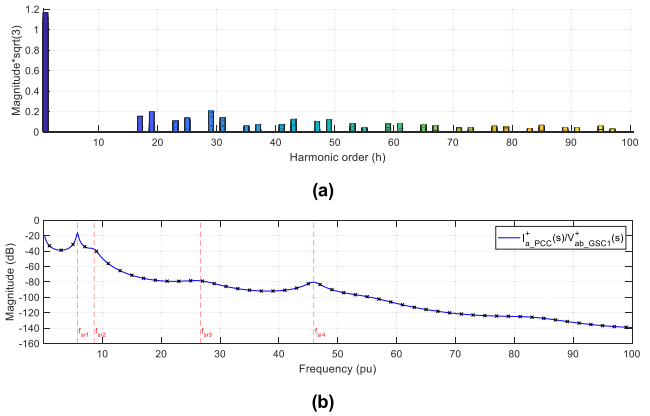

FIGURE 18. Risk of amplification of harmonics for GSCs using SHE-PWM modulation. (a) SHE-PWM line-to-line spectrum with different m_a values stacked. (b) Bode plot of transfer function $I^{+}_{a\_PCC}(s)/V^{+}_{ab\_GSC1}(s)$.

Fig. 18(a) shows the SHE-PWM spectrum of the voltage signal $v_{ab\_GSCi}(t)$ in a 2D-plane for different m_a values. Fig. 18(b) depicts the Bode plot of transfer function $I^{+}_{a\_PCC}(s)/V^{+}_{ab\_GSC1}(s)$, which is also valid for the negative-sequence.

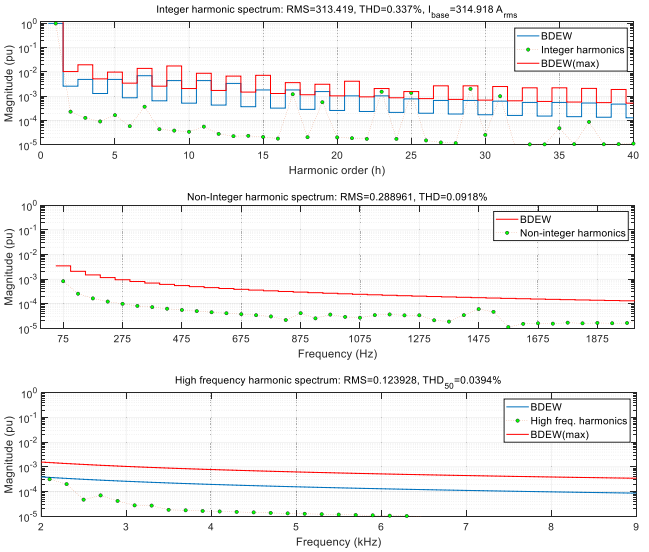

FIGURE 19. Harmonic spectrum of current signal $i_{a\_PCC}(t)$ plotted against the BDEW harmonic current limits at PCC point (SCR = 20). This scenario considers WTs operating at rated condition (wind direction = west, wind speed = 24 m/s), $V_{bus} = 5700\ V$, $m_a \approx 0.91$ and SHE-PWM modulation.

As depicted in Fig. 18, the first two resonances do not represent an issue with respect to non-compliance of harmonic limits since low order harmonics are not injected.

On the other hand, there is a possibility of infringing the BDEW limits of injected harmonics that are close to resonances f_{sr3} and f_{sr4}. These hypotheses shall be corroborated by means of the Simulink®-based model and the wind conditions addressed in section II.

Fig. 19 shows the harmonic spectrum of the current signal $i_{a\_PCC}(t)$ at rated condition. The figure also shows the current-harmonic limits imposed by the BDEW grid code at PCC point.

Table 20 gives a summary of the fulfillment of the grid code for different operating points considering several wind speeds and directions.

According to Fig. 19 and Table 20, the BDEW grid code is fulfilled for the evaluated operating points since there are no infringement of the technical rules pointed out in section II.

Even though the BDEW grid code is fulfilled, it is important to be aware of harmonics of order 23rd, 25th and 29th since exceeding the BDEW(max) curve will provoke the non-fulfillment of the grid code.

Table 21 gives the total harmonic distortion (THDi) values of the current-signal $i_{a\_PCC}(t)$ for WTs operating with SHE-PWM and for different operating points.

In general, the THDi values for the low- and high-frequency harmonic subgroups are reduced for SHE-PWM if compared with CB-PWM modulation. Contrasting the THDi values of both modulation strategies for a wind speed of 24 m/s, the THDi value for the low-frequency subgroup is reduced from 2.28% to a value of 0.34%.

TABLE 20. Compliance of the BDEW grid code at OWPP level for SHE-PWM and for different operating points.

Wind Condition		BDEW Comp.	Harmonic (h)	Infringement of BDEW limits for harmonics of order:		
				$6n \pm 1$ with $n = 1 \cdots 4$	Others	Inter-harmonic
Dir.	m/s		>BDEW limit	>200% BDEW limit	>400% BDEW limit	>BDEW limit
W	24	Yes	23, 25, 29, 31	–	–	–
	16	Yes	29	–	–	–
	12.5	Yes	–	–	–	–
	8	Yes	23, 25, 29, 31	–	–	–
NW	24	Yes	23, 25, 29, 31	–	–	–
	16	Yes	23, 25, 29, 31	–	–	–
	12.5	Yes	–	–	–	–
	8	Yes	23, 25, 29, 31	–	–	–
N	24	Yes	23, 25, 29, 31	–	–	–
	16	Yes	–	–	–	–
	12.5	Yes	29	–	–	–
	8	Yes	23, 25, 29, 31	–	–	–

TABLE 21. Total harmonic distortion at OWPP level for SHE-PWM and for different operating points.

Wind Condition		Low Frequency		Interharmonics		High Frequency	
Dir.	Speed (m/s)	RMS (A)	THDi (%)	RMS (A)	THDi (%)	RMS (A)	THDi (%)
W	24	313.42	0.34	0.289	0.0918	0.1239	0.039
	16	264.88	0.17	0.243	0.0773	0.0756	0.024
	12.5	188.04	0.11	0.173	0.055	0.0681	0.022
	8	83.43	0.31	0.106	0.0338	0.0773	0.025
NW	24	313.42	0.34	0.289	0.0918	0.1239	0.039
	16	301.06	0.30	0.276	0.0881	0.0967	0.031
	12.5	240.82	0.13	0.221	0.0702	0.0508	0.016
	8	92.37	0.32	0.093	0.0295	0.0892	0.028
N	24	301.02	0.32	0.278	0.0881	0.1036	0.033
	16	216.74	0.11	0.199	0.0632	0.0831	0.026
	12.5	153.58	0.14	0.141	0.0449	0.0481	0.015
	8	78.16	0.3	0.131	0.0416	0.0689	0.022

As inferred from the data presented in Table 21, the THDi values of low- and high-frequency harmonics are lower for operating points having wind speeds equal to 12 m/s and 16 m/s. On the contrary, the THDi values of interharmonics increase by increasing the active power delivered by the OWPP.

Finally and due to the reasons stated in this section, it can be pointed out that this particular solution of SHE-PWM is suitable to be used for this OWPP scenario.

B. SHE-PWM ORIENTED TECHNIQUES TO FURTHER IMPROVE POWER QUALITY

There are three clear complementary solutions to further improve the power quality with SHE-PWM. The first is by means of adding switching angles in order to eliminate, for example, harmonics approaching the maximum limit restricted by the grid code, e.g., the harmonic of order 25th depicted in Fig. 19. Even though this technique is the most evident, it brings two clear consequences. These are increased switching losses of the power converter and the complexity of finding a continuous solution over a wide range of amplitude modulation indexes. This solution is not addressed in this paper.

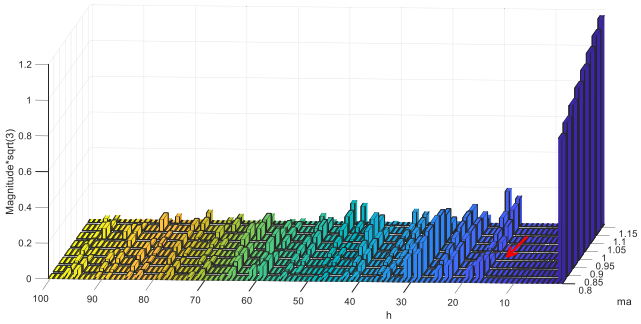

FIGURE 20. Harmonic spectrum of SHE-PWM modulation for amplitude modulation indexes ranging from 0.8 to 1.16, approximately.

The second solution is by means of changing the operating point of wind turbines, which can be implemented by changing the DC-link voltage setpoint of the GSC of each WT, the reactive power setpoint of each WT, or a combination of both strategies. This is done with the aim of operating with amplitude modulation indexes that result in a lower harmonic distortion level or in the reduction of specific harmonics at the PCC point of the OWPP. Examples of harmonics to reduce are:

- Harmonics that exceed the limits imposed by the grid code.
- Low order harmonics.
- Harmonics amplified by the electrical infrastructure of the OWPP.

Considering the previous ideas, it is important to analyze in detail the harmonic spectrum of the particular solution of SHE-PWM that has been implemented. Fig. 20 shows the harmonic spectrum for this type of modulation and for m_a values ranging from 0.8 to 1.16, approximately.

As depicted in Fig. 20, the harmonic emission of the OWPP base scenario can be reduced if the GSC of each wind turbine operates around an amplitude modulation index of 0.96. The reason for this statement is that harmonics of order 17th and 19th have small magnitudes for m_a values around 0.96.

Additionally, the magnitude of harmonics of order 23rd, 25th, 29th, 31st, 35th, 37th, and 41st barely change when compared with m_a values around 0.91. Despite these aspects, it is still required to evaluate the compliance of the BDEW grid code for the scenario to study and if any other factor could make this idea to be rejected.

Finally, the improvement of the harmonic distortion can be tackled by considering the redesign of the GSC connection filter according to the harmonic spectrum of the considered

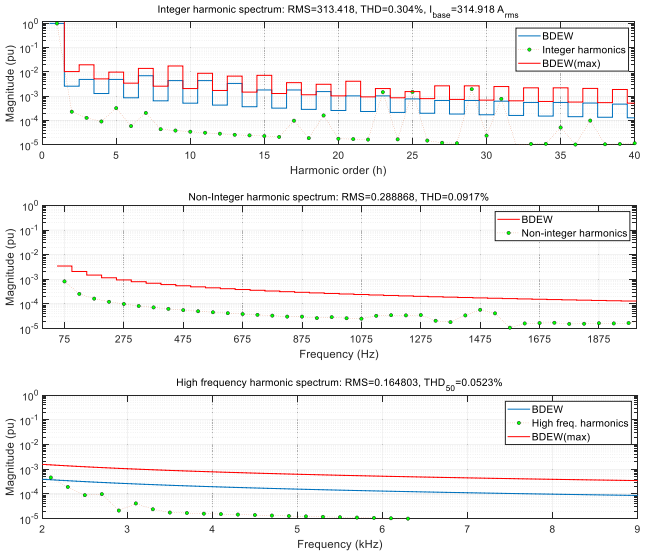

FIGURE 21. Harmonic spectrum of current signal $i_{a\_PCC}(t)$ plotted against the BDEW harmonic current limits at PCC point (SCR = 20). This scenario considers WTs operating at rated condition (wind direction = west, wind speed = 24 m/s), SHE-PWM modulation and the change of the DC-link voltage setpoint of GSCs.

SHE-PWM modulation. Two case studies are given next to exemplify the previous proposals.

1) CHANGE OF THE DC-LINK VOLTAGE SETPOINT

For this complementary solution, the DC-link voltage is modified with a low ramp variation, under certain limits, until reaching the desired setpoint. The idea is to increase the amplitude modulation index from a value of 0.91 to an approximate value of 0.96. This is done by decreasing the setpoint of the DC-link voltage of the GSCs from 5700 V, previous scenarios, to a voltage of 5400 V.

Fig. 21 shows the harmonic spectrum of the current signal $i_{a\_PCC}(t)$ for this case study at the rated condition. The figure also shows the current-harmonic limits imposed by the BDEW grid code at PCC point.

According to this figure, the compliance of the BDEW grid code is fulfilled since the limits imposed by the BDEW regulations are not infringed. Low frequency harmonics, interharmonics and high frequency harmonics lay within the allowable limits.

Table 22 shows a comparison of the THDi values for this case study and previous scenarios. To give an example, the THDi value for the low frequency subgroup is reduced from a value of 0.337% to a value of 0.304%. On the contrary, the THDi value of high frequency components increased from a value of 0.039% to a value of 0.052%.

Fig. 22 aids in the visualization of the previous comparison by depicting the harmonic spectrum of the current signal for the last two case studies and by showing how targeted harmonics, i.e., 17th and 19th harmonic, are reduced. For example, the harmonic of order 17th is reduced from a value of 0.12% to a value of 0.01%. For the case of harmonic 19th, this is reduced from a value of almost 0.06% to a value of 0.017%.

TABLE 22. Comparison of the THD values at PCC point for GSCs operating with a DC-link bus voltage of 5400 v and previous scenarios.

Scenario	Low-Freq.		Interharmonics		High-Freq.	
	RMS Value (A)	THDi (%)	RMS Value (A)	THDi (%)	RMS Value (A)	THDi (%)
CB-PWM $V_{bus} = 5700\,V$	313.495	2.28	0.293	0.093	0.767	0.244
SHE-PWM $V_{bus} = 5700\,V$	313.419	0.337	0.288	0.091	0.124	0.039
SHE-PWM $V_{bus} = 5400\,V$	313.418	0.304	0.288	0.091	0.165	0.052

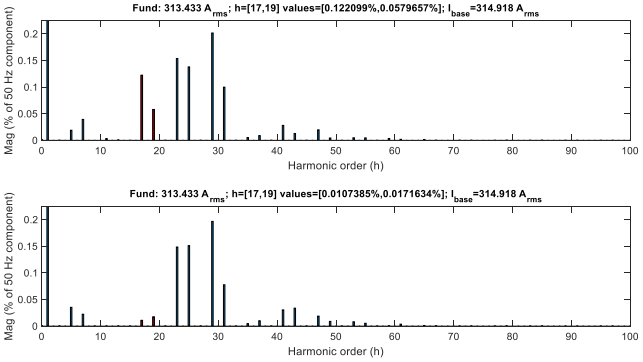

FIGURE 22. Harmonic comparison of current signal $i_{a\_PCC}(t)$. The top figure represents the case study considering SHE-PWM and $V_{bus} = 5700\,V$. The bottom figure represents the case study considering SHE-PWM and $V_{bus} = 5400\,V$.

TABLE 23. Parameters of the redesigned GSC connection filter.

Parameter	Value
Converter side inductance (L_c)	675 µH
Filter capacitance (C_f)	365 µF
Damping circuit resistance (R_d)	50 Ω
Damping circuit inductance (L_d)	95 µH

Before continuing with the next complementary solution, it is important to point out that even though the results for this case study are only presented at the rated condition but they were also tested at other operating points. BDEW grid code is fulfilled for these other operating points as well.

2) REDESIGN OF THE GSC CONNECTION FILTER

For this complementary solution, the GSC connection filter is redesigned by taking into account the harmonic spectrum of SHE-PWM modulation. The redesign of the LCL-rl filter is performed by following the methodology presented in reference [19] and depicted in Fig. 23.

Table 23 gives the parameters of the GSC connection filter that is redesigned by taking into account the previous procedure.

Fig. 24 shows the SHE-PWM spectrum and the Bode plot of the transfer function $I^{+}_{a\_PCC}(s)/V^{+}_{ab\_GSC1}(s)$, which is also valid for the negative-sequence. The SHE-PWM spectrum is depicted for several stacked m_a values.

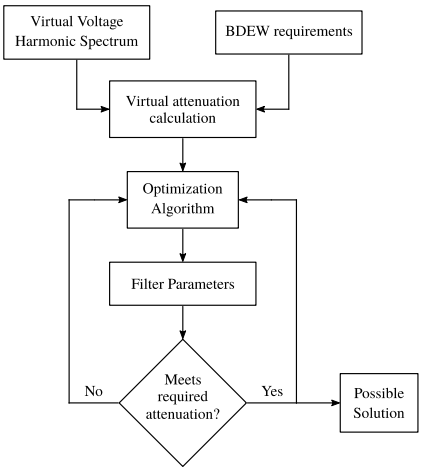

FIGURE 23. Methodology for the design of the GSC connection filter. Source [19].

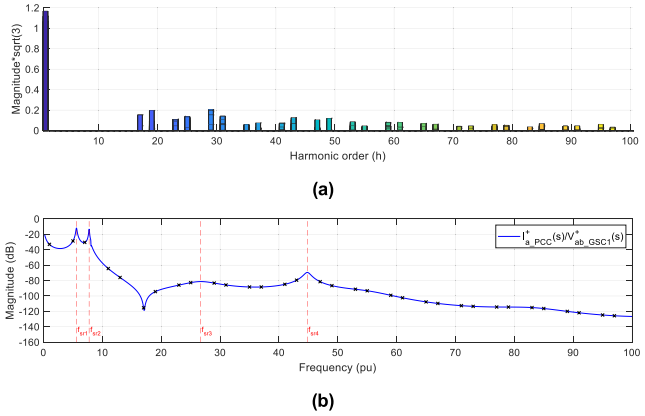

FIGURE 24. Risk of amplification of harmonics for GSCs using SHE-PWM modulation and redesigned filter. (a) SHE-PWM line-to-line spectrum with different m_a values stacked. (b) Bode plot of transfer function $I^{+}_{a\_PCC}(s)/V^{+}_{ab\_GSC1}(s)$.

As shown in Fig. 24(b), the GSC connection filter is designed so that the resonance frequency (new f_{sr2}) lays close to the harmonic of order 9th. This is done to guarantee that no harmonic excitation is possible since the modulation eliminates the surrounding harmonics. Furthermore, the LCL-rl filter is designed so that the anti-resonant frequency lays on the 17th harmonic, which is the first non-eliminated harmonic that appears in the current. The attenuation level for this harmonic is high, almost equal to -120 dB.

Fig. 25 shows the harmonic spectrum of the current-signal $i_{a\_PCC}(t)$ at the PCC point and at the rated condition. The figure also shows the current-harmonic limits imposed by the BDEW grid code. According to this figure, the compliance of the BDEW grid code is fulfilled since the restrictions for certification approval are not infringed. Integer harmonics, interharmonics and high frequency harmonics lay within the allowable limits. Even though the results for this case study are only presented at rated condition but they were also tested at other operating points. BDEW grid code is fulfilled for other operating points as well.

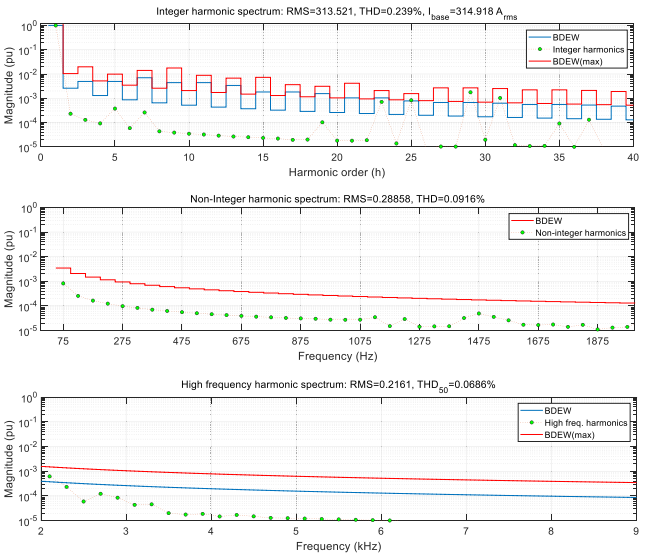

FIGURE 25. Harmonic spectrum of current signal $i_{a\_PCC}(t)$ plotted against the BDEW harmonic current limits at PCC point (SCR = 20). This scenario considers WTs operating at rated condition (wind direction = west, wind speed = 24 m/s), $V_{bus} = 5700\ V$, $m_a \approx 0.91$, SHE-PWM modulation and the redesign of the GSC connection filter.

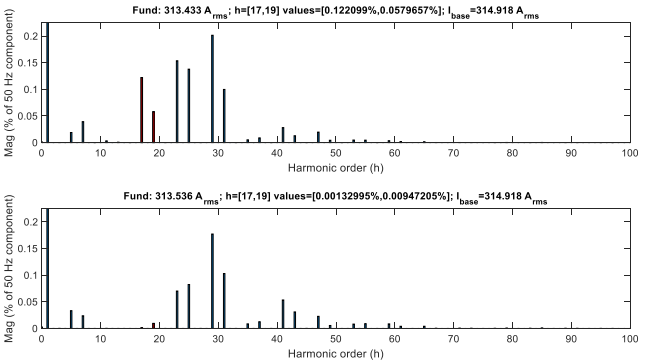

FIGURE 26. Harmonic comparison of current signal $i_{a\_PCC}(t)$. The top figure represents the case study considering SHE-PWM, initial GSC connection filter, and $V_{bus} = 5700\ V$. The bottom figure represents the case study considering SHE-PWM, redesigned filter, and $V_{bus} = 5700\ V$.

Fig. 26 shows the spectrum of the current-signal $i_{a\_PCC}(t)$ for this scenario and for the last 20 ms time window, for better visualization. As expected, harmonics of order 17th and 19th (red bars) are highly reduced compared to the first case study considering SHE-PWM modulation, initial GSC connection filter and a DC-link voltage of 5700 V.

Table 24 gives the THDi values of the current-signal $i_{a\_PCC}(t)$. This table also provides the THDi values of previous cases for comparative purposes. It is shown that lower THDi values are obtained when considering the SHE-PWM oriented filter.

The THDi value of the low frequency subgroup is further reduced to a value of 0.239%. An improvement of 2.041% is achieved in comparison with the scenario in which the WTs operate with a typical CB-PWM modulation.

Finally, it is worth to point out that the solution evaluated in this last case study is the most feasible among the presented

TABLE 24. Comparison of the THD values at PCC point for the redesign of the GSC connection filter and previous scenarios.

Scenario	Low Freq.		Interharmonics		High Freq.	
	RMS Value (A)	THDi (%)	RMS Value (A)	THDi (%)	RMS Value (A)	THDi (%)
CB-PWM $V_{bus} = 5700\,V$	313.495	2.28	0.293	0.093	0.767	0.244
SHE-PWM $V_{bus} = 5700\,V$	313.419	0.337	0.288	0.091	0.124	0.039
SHE-PWM $V_{bus} = 5400\,V$	313.418	0.304	0.288	0.091	0.165	0.052
SHE-PWM Redesign filter $V_{bus} = 5700\,V$	313.521	0.239	0.288	0.091	0.216	0.068

ones in terms of harmonic distortion levels, BDEW grid code compliance, and complexity.

VI. ROBUSTNESS EVALUATION DUE TO PARAMETER UNCERTAINTY

The aim of this section is to carry out the robustness evaluation due to parameter uncertainty for the WT oriented solutions proposed in this article.

To address this objective, two main aspects are analyzed. First, changes in Bode plots of the transfer function $I^+_{a\_PCC}(s)/V^+_{ab\_GSC1}(s)$, shown in previous sections, are presented due to parameter variation of the main power components of the OWPP. This is performed to have a general idea on how the variation of these parameters changes the frequency value of resonances (f_{sr1} to f_{sr4}), the "new" attenuation level that will see each harmonic and the way harmonics of the same order are added at the PCC point of the OWPP.

As second aspect, the evaluation of harmonics is performed for an SCR value of five, probing that the implemented control loops and the particular solution of SHE-PWM proposed in section V give good results in terms of harmonic compliance even when considering the connection of the OWPP to a relatively weak grid.

A. CHANGES IN BODE PLOTS DUE TO PARAMETER VARIATION

Fig. 27 to Fig. 29 depict the changes in studied Bode plots when varying the parameters of the GSC connection filter, the capacitance values of both types of submarine cables, and the short-circuit impedance of the grid (or SCR). Even though the changes in Bode plots are shown for the positive-sequence, they are also valid for the negative-sequence.

It is worth to point out that the changes depicted next are in agreement with the information given by the participation factors in Table 16. It is also important to take into account in conjunction with these Bode plots, the harmonic spectrum of SHE-PWM strategy, already shown in Fig. 18(a), to predict the risk of harmonic amplification and the eventual infringement of the BDEW grid code.

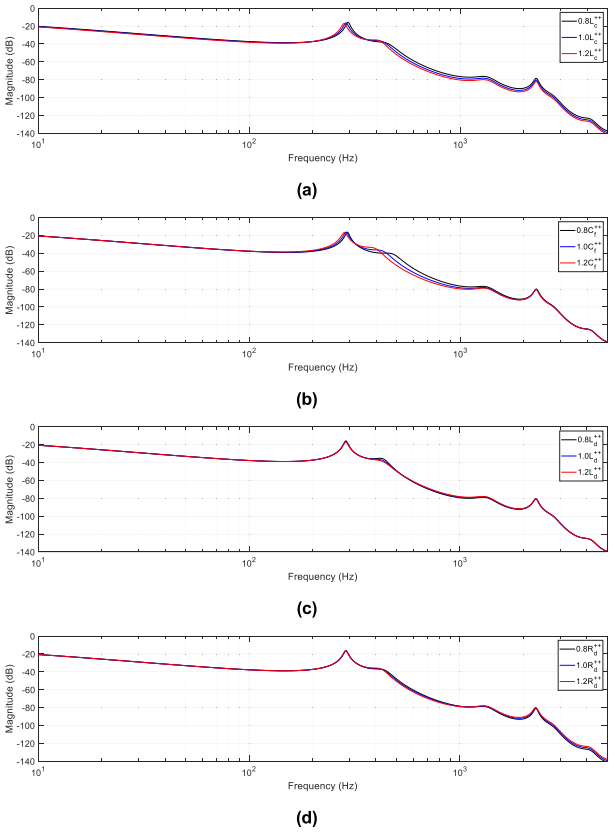

FIGURE 27. Changes in Bode plots of the transfer function $I^+_{a\_PCC}(s)/V^+_{ab\_GSC1}(s)$ due to a variation of GSC connection filter parameters. (a) L_c value. (b) C_f value. (c) L_d value. (d) R_d value.

Fig. 27 shows the changes in Bode plots due to a variation of ±20% of the GSC connection filter parameters of Table 5.

Fig. 27(a) shows the effect of varying the filter inductance L_c on the first four series resonances. Regarding the frequency variation, series resonance f_{sr1} decreases while increasing the inductance value. The maximum variation is lower than 10 Hz. On the other hand, series resonance f_{sr2} is the one that exhibits the highest change, a maximum variation of approximately 20 Hz. This series resonance decreases while increasing the inductance value. Finally, the frequency values of remaining resonances barely change. Regarding the level of attenuation, not big changes are noticed.

Fig. 27(b) shows the effect of varying the filter capacitance C_f on the first four series resonances. Regarding the frequency variation, series resonance f_{sr2} is the one that exhibits the highest change, a maximum variation of approximately 50 Hz. This series resonance decreases while increasing the capacitance value. Remaining series resonances barely change in both magnitude and frequency.

The Bode plots shown in Fig. 27(c) and (d) barely change. It can be inferred from previous points that no changes in comparison with the ones obtained in subsection V.A are expected for the filter variations evaluated previously.

Fig. 28 shows the changes in Bode plots due to a variation of ±20% of the capacitance values of the submarine cables given in Table 9 and Table 10.

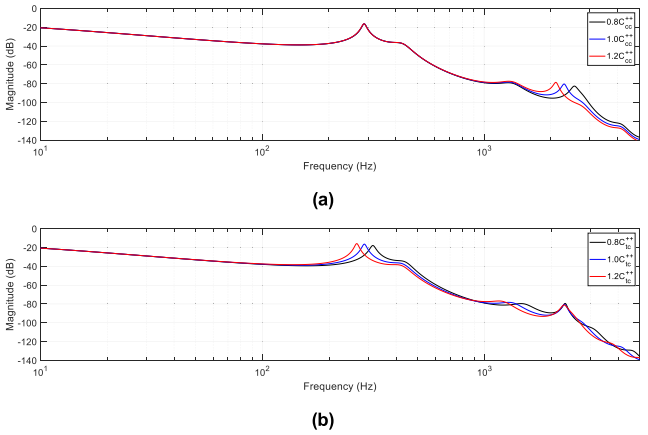

FIGURE 28. Changes in Bode plots of the transfer function $I^+_{a\_PCC}(s)/V^+_{ab\_GSC1}(s)$ due to the variation of the capacitance of submarine cables. (a) Capacitance C_{cc} of the MVAC submarine cables (b) Capacitance C_{tc} of the HVAC submarine cable.

Fig. 28(a) shows the effect of varying the capacitance C_{cc} value on the first four series resonances. Regarding the frequency variation, series resonance f_{sr4} is the one that exhibits the highest change, a maximum variation of approximately 250 Hz. This series resonance decreases while increasing the capacitance value. Remaining series resonances barely change in both magnitude and frequency.

It can be inferred from previous reasons that no changes in comparison with the ones obtained in subsection V.A are expected for this case for harmonics of order lower than 40. For harmonics of order 40 to 60, changes in their magnitudes are expected in comparison with the ones obtained in subsection V.A.

For the case of Fig. 28(b), there is not risk of harmonic amplification since low order harmonics around the first series resonance f_{sr1} are not injected by particular solution of SHE-PWM presented in section V. The main concern is to ensure the stability of the system since the low frequency value of resonance f_{sr1}, around 260 Hz (red line) and even lower for other cases, can affect the bandwidth of the WT control loops and make the system unstable if it is not properly tuned.

In this sense and in order to guarantee the stability of the system, two possible actions can be employed:

- A reduction of the bandwidth of the WT control loops (current-control bandwidth, PLL bandwidth, measurement filters bandwidth, etc.). The main drawback of this strategy is that the dynamic behavior of the system will be slower. This is that the settling time and rising time will be increased which is not always an option.
- The implementation of advanced control structures such as active damping strategies.

Fig. 29 shows the changes in Bode plots due to a variation of the SCR value. The SCR value is varied from a value of 20 to a value of five with an additional middle value of 10. An SCR equal to 20 represents a strong grid while an SCR value of five represents a relatively weak grid [37].

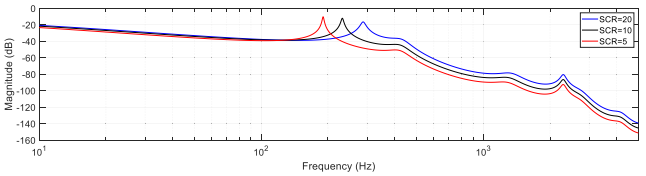

FIGURE 29. Changes in Bode plots of the transfer function $I^+_{a\_PCC}(s)/V^+_{ab\_GSC1}(s)$ due to a variation of the short circuit ratio (SCR) of the power grid.

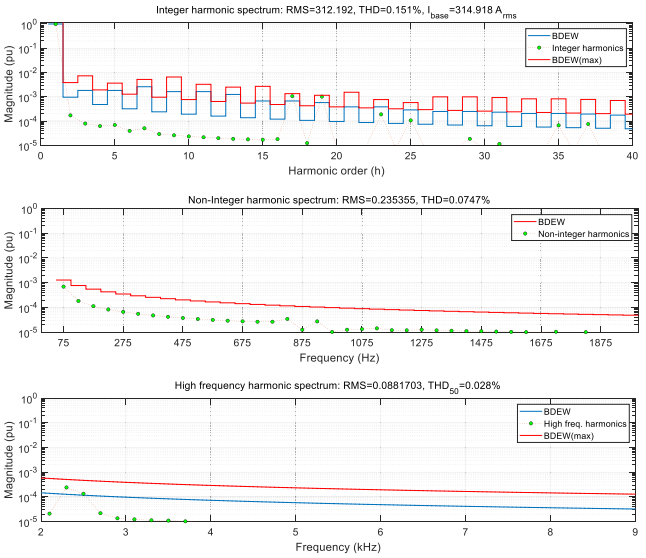

FIGURE 30. Harmonic spectrum of current signal $i_{a\_PCC}(t)$ plotted against the BDEW harmonic current limits at PCC point (SCR = 5). This scenario considers WTs operating at rated condition (wind direction = west, wind speed = 24 m/s), $V_{bus} = 5700\ V$, $m_a \approx 1.15$, SHE-PWM modulation, and GSC connection filter values of Table 5.

In general, it can be concluded that connecting the OWPP base scenario to a weak grid tends to locate the resonance f_{sr1} to lower frequency values. This resonance is shifted in frequency from a value of 287.88 Hz to an approximate value of 190 Hz for the variations evaluated.

To evaluate the harmonic compliance of this last case, the BDEW harmonic limits needs to be updated according to the information presented in subsection II.B since the SCR value has changed.

For the scenarios presented in Fig. 28(b) and Fig. 29, time-domain simulations must be run to take into account both, stability and harmonic compliance of the grid codes. It is not an easy task to predict the expected outcome as in comparison with the conclusions stated for Fig. 27.

B. HARMONIC EVALUATION OF THE OWPP BASE SCENARIO WITH SCR = 5

In order to perform the harmonic evaluation of the OWPP base scenario with a SCR value of five, time-domain simulations are run to verify the fulfillment of the BDEW grid code in terms of harmonics.

Fig. 30 shows the harmonic spectrum of the current-signal $i_{a\_PCC}(t)$ at the PCC point and as close as possible to the rated condition. The figure also shows the updated current-harmonic limits imposed by the BDEW grid code when

considering a SCR value of five. According to this figure, the compliance of the BDEW grid code is fulfilled since the restrictions for certification approval are not infringed.

Integer harmonics, interharmonics and high frequency harmonics lay within the allowable limits.

Even though the compliance of the BDEW grid code is fulfilled, it is important to note that harmonics of order 17 and 19 are very close to the maximum allowable limits. This should be considered as a warning message and an aspect to further improve.

VII. CONCLUSION

This paper has presented the harmonic evaluation of an OWPP scenario. It is worth to point out that the studies and the modeling approach presented in this paper serve as a generic simulation tool for stakeholders within the wind power industry, to conduct harmonic studies and evaluate the grid code compliance of an OWPP from a power quality perspective and during its design stage. The following conclusions can be pointed out regarding the studies carried out.

First and in general terms, the harmonic assessment must be carried out not only at wind turbine level but also at wind power plant level, i.e., at the PCC point of the OWPP, and for different operating points, active- and reactive-power references.

As presented in section IV-A for WTs operating with the commonly used CB-PWM modulation, the harmonic evaluation at WT level results in the local compliance of the BDEW grid code. However, the fulfillment of the grid code might not be achieved for several operating points when performing the harmonic evaluation of an OWPP with resonances at low frequency values. Thus, additional wind turbine analyses for specific applications (i.e. wind farm layout, transmission link distance, short-circuit ratio of the grid, and other characteristics of the electrical network) are needed.

An example of the aforementioned situation has been carried out in section IV-B where the compliance of the BDEW grid code at the PCC point of the OWPP base scenario is not achieved. For this scenario, three important factors heavily affect the current harmonic emission and the compliance of the BDEW grid code.

First, the magnitude of the harmonics injected by the GSCs. Second, the attenuation level of the system around these harmonics, especially if a resonance matches or is close to a certain harmonic or harmonics. Third, the way harmonics of the same order are added at a specific point of the OWPP. The summation of harmonics depends mainly on the operating point of the wind turbines and the phase shift of the electrical infrastructure of the OWPP that sees each WT.

To improve the harmonic emission of the OWPP and the compliance of the grid code in terms of harmonics, WT oriented solutions have been presented in this paper. The implementation of a particular solution of SHE-PWM modulation has been presented together with complementary solutions to further improve the harmonic emission of the OWPP. This type of modulation strategy is more suited to be used in scenarios of OWPPs having resonances at low-frequency values (around 100 Hz to 400 Hz), as the analyzed. The robustness evaluation is done showing that for a SCR value of five (weak grid), the solution proposed in this article still meets the grid code in terms of harmonics.

Even though, this robustness evaluation is met for other conditions, there are open problems and future issues that the authors encourage their further investigation. One of them is the evaluation and comparison of other modulation schemes of the WTs, such as Selective Harmonic Mitigation (SHM-PWM) which reduces, does not eliminates, the magnitude of a greater number of harmonics for a given number of transition angles.

Another aspect to focus on is the design of advanced WT control strategies that ensure the stability of the system for a wider range of parameter variations and mainly when the OWPP is connected to an extremely weak grid or when the perturbation capability of the OWPP cannot be neglected.

As last point and mixing the previous two aspects, the design of an upper level algorithm implemented in the wind turbines that automatically changes the modulation strategy and/or tunes the control loops to achieve stability and to meet grid code requirements in terms of harmonics.

REFERENCES

[1] L. H. Kocewiak, *Harmonics in Large Offshore Wind Farms*. Aalborg, Denmark: Aalborg Univ., 2012.

[2] I. Erlich, F. Shewarega, C. Feltes, F. W. Koch, and J. Fortmann, "Offshore wind power generation technologies," *Proc. IEEE*, vol. 101, no. 4, pp. 891–905, Jan. 2012.

[3] T. Ackermann, *Wind Power in Power Systems*, 2nd ed. Hoboken, NJ, USA: Wiley, 2012.

[4] D. Xu, F. Blaabjerg, W. Chen, and N. Zhu, *Advanced Control of Doubly Fed Induction Generator for Wind Power Systems*, 1st ed. Hoboken, NJ, USA: Wiley, 2018.

[5] L. Sainz, L. Monjo, J. Pedra, M. Cheah-Mane, J. Liang, and O. Gomis-Bellmunt, "Effect of wind turbine converter control on wind power plant harmonic response and resonances," *IET Electr. Power Appl.*, vol. 11, no. 2, pp. 157–168, Feb. 2016.

[6] S. Zhang, S. Jiang, X. Lu, B. Ge, and F. Z. Peng, "Resonance issues and damping techniques for grid-connected inverters with long transmission cable," *IEEE Trans. Power Electron.*, vol. 29, no. 1, pp. 110–120, Jan. 2014.

[7] J. B. Glasdam, "Harmonics in offshore wind power plants employing power electronic devices in the transmission system," Aalborg Univ., Aalborg, Denmark, Tech. Rep., 2015.

[8] H. Kocewiak, J. Hjerrild, and C. L. Bak, "Wind turbine converter control interaction with complex wind farm systems," *IET Renew. Power Gener.*, vol. 7, no. 4, pp. 380–389, Jul. 2013.

[9] E. Ebrahimzadeh, F. Blaabjerg, T. Lund, J. G. Nielsen, and P. C. Kjær, "Modelling and stability analysis of wind power plants connected to weak grids," *Appl. Sci.*, vol. 9, no. 21, p. 4695, Nov. 2019.

[10] Z. Liu, J. Rong, G. Zhao, and Y. Luo, "Harmonic assessment for wind parks based on sensitivity analysis," *IEEE Trans. Sustain. Energy*, vol. 8, no. 4, pp. 1373–1382, Oct. 2017.

[11] K. Yang, "On harmonic emission, propagation and aggregation in wind power plants," Lulea Univ. Technol., Luleå, Sweden, Tech. Rep., 2015.

[12] C. Ruiz, M. Zubiaga, G. Abad, D. Madariaga, and J. Arza, "Validation of a wind turbine harmonic model based on the generic type 4 wind turbine Standard," in *Proc. 20th Eur. Conf. Power Electron. Appl.*, 2018, p. 10.

[13] C. Ruiz, G. Abad, M. Zubiaga, D. Madariaga, and J. Arza, "Frequency-dependent Pi model of a three-core submarine cable for time and frequency domain analysis," *Energies*, vol. 11, no. 10, p. 2778, Oct. 2018.

[14] *Fact-Sheet Alpha Ventus*, Alphaventus, 2015.

[15] M. Zubiaga, G. Abad, and J. A. Barrena, *Energy Transmission and Grid Integration of AC Offshore Wind Farms*. Rijeka, Croatia: InTech, 2012.

[16] *Technical Guideline—Generating Plants Connected to the Medium-Voltage Network*, BDEW, Berlin, Germany, 2008.
[17] *Rules and Transitional Periods for Specific Requirements Complementary to the Technical Guideline?: Generating Plants Connected to the Medium-Voltage Network—Guideline for Generating Plants' Connection to and Parallel Operation With the Medium-Voltage*, BDEW, Berlin, Germany, 2013.
[18] M. Bradt, B. Badrzadeh, E. Camm, D. Mueller, J. Schoene, T. Siebert, T. Smith, M. Starke, and R. Walling, "Harmonics and resonance issues in wind power plants," in *Proc. PES T&D*, May 2012, pp. 1–8.
[19] M. Zabaleta, E. Burguete, D. Madariaga, I. Zubimendi, M. Zubiaga, and I. Larrazabal, "LCL grid filter design of a multimegawatt medium-voltage converter for offshore wind turbine using SHEPWM modulation," *IEEE Trans. Power Electron.*, vol. 31, no. 3, pp. 1993–2001, Mar. 2016.
[20] N. Chiesa and B. Gustavsen, "Frequency-dependent modeling of transformer winding impedance from $R(w)$/L measurements," *IEEE Trans. Power Deliv.*, vol. 29, no. 3, pp. 1511–1513, Feb. 2014.
[21] *Submarine Power Cables*, Nexans, Paris, France, 2013.
[22] *XLPE Submarine Cable Systems*, ABB, Zürich, Switzerland, 2014.
[23] *National Grid ESO, Electricity Ten Year Statement 2012, Appendix E: Technology Sheets*. 2012.
[24] M. De-Prada-Gil, C. G. Alías, O. Gomis-Bellmunt, and A. Sumper, "Maximum wind power plant generation by reducing the wake effect," *Energy Convers. Manage.*, vol. 101, pp. 73–84, Sep. 2015.
[25] R. J. Barthelmie, G. C. Larsen, S. T. Frandsen, L. Folkerts, K. Rados, S. C. Pryor, B. Lange, and G. Schepers, "Comparison of wake model simulations with offshore wind turbine wake profiles measured by sodar," *J. Atmos. Ocean. Technol.*, vol. 23, no. 7, pp. 888–901, Jul. 2006.
[26] N. O. Jensen, "A note on wind generator interaction," Tech. Rep., 1983, pp. 1–16.
[27] M. Thørgersen, T. Sørensen, and P. Nielsen, "WindPRO/PARK: Introduction to wind turbine wake modelling and wake generated turbulence," Tech. Rep., 2005.
[28] I. Katic, J. Hojstrup, and N. O. Jensen, "A simple model for cluster efficiency," in *Proc. EWEC*, vol. 1, 1986, pp. 407–410.
[29] AlphaVentus. (2019). *Alpha Ventus*. [Online]. Available: https://www.alpha-ventus.de/english
[30] A. Westerhellweg, B. Cañadillas, F. Kinder, and T. Neumann, "Wake measurements at alpha ventus–dependency on stability and turbulence intensity," *J. Phys., Conf. Ser.*, vol. 555, Dec. 2014, Art. no. 012106.
[31] A. Westerhellweg, B. Canadillas, F. Kinder, and T. Neumann, "Detailed analysis of offshore wakes based on two years data of alpha ventus and comparison with CFD simulations," *DEWI Mag.*, vol. 22, no. 42, p. 7, 2013.
[32] G. Verghese, I. Perez-Arriaga, and F. Schweppe, "Selective modal analysis with applications to electric power systems, Part II: The dynamic stability problem," *IEEE Trans. Power App. Syst.*, vol. PAS-101, no. 9, pp. 3126–3134, Sep. 1982.
[33] I. Perez-Arriaga, G. Verghese, and F. Schweppe, "Selective modal analysis with applications to electric power systems, PART I: Heuristic introduction," *IEEE Trans. Power App. Syst.*, vols. PAS–101, no. 9, pp. 3117–3125, Sep. 1982.
[34] B. Wu, *High-Power Converters and AC Drives*. Hoboken, NJ, USA: Wiley, 2006.
[35] E. F. Fuchs and M. Masoum, *Power Quality in Power Systems and Electrical Machines*, 2nd ed. New York, NY, USA: Academic, 2015.
[36] F. Blaabjerg, *Control of Power Electronic Converters and Systems*, vol. 1. New York, NY, USA: Academic, 2018.
[37] M. Gupta, A. Martinez, and S. Saylors, "Experiences with wind power plants with low SCR," Tech. Rep., Mar. 2015, pp. 1–24.

CARLOS RUIZ was born in Managua, Nicaragua, in 1989. He received the M.Sc. degree in power electronics and the Ph.D. degree in electrical engineering from Mondragon University, Spain, in 2015 and 2020, respectively.

He worked as a part-time Teacher with the Electronics Department, National University of Engineering, Nicaragua, in 2012, 2013, and 2016. In 2020, he joined the Electronics and Computer Department, Mondragon University. His main research interests include the harmonic evaluation and stability analysis of electrical power systems, mainly offshore wind power plants.

GONZALO ABAD received the degree in electrical engineering from Mondragon University, in 2000, the M.Sc. degree in advanced control from The University of Manchester, U.K., in 2001, and the Ph.D. degree in electrical engineering from Mondragon University, in 2008.

He joined the Electronics and Computing Department, Mondragon University, in 2001. He has coauthored several articles, patents, and books in the areas of wind power generation, multilevel power converters, and control of electric drives. His main research interests include renewable energies, power conversion, and motor drives.

MARKEL ZUBIAGA received the M.Sc. degree in electrical engineering and the Ph.D. degree from Mondragon University, Spain, in 2005 and 2011, respectively.

Since 2011, he has been working as a Research and Development Engineer with the Renewable Energy Systems Department, Ingeteam. His research interests include power electronics, wind power, grid forming control, and energy transmission systems.

DANEL MADARIAGA was born in Bilbao, Spain, in 1973. He received the M.Eng. degree in industrial engineering from the University of the Basque Country, Bilbao, in 1998, and the M.Sc. degree in physics from UNED, Madrid, Spain, in 2008.

In 1998, he joined the Research and Development Department, Ingeteam Technology, S.A., Zamudio, Spain, where he was mainly involved in research on high-power inverters, especially on vector control, firmware design and programming, mathematical modeling, space-vector pulsewidth modulation (PWM), and three-level neutral-point-clamped inverters. His current research interests include solving the polynomial equation systems appearing in selective harmonic elimination PWM techniques, and modulation techniques for balancing the dc bus of 3-L NPC inverters.

JOSEBA ARZA received the B.Sc. degree in power electronics from the University of Mondragon, Spain, in 1994, the M.Sc. degree in electric machines from the École Nationale Supérieure d'Ingénieurs Électriciens de Grenoble, France, in 1996, and the Ph.D. degree in drives control and regulation from the Institut National Polytechnique de Grenoble, France, in 1999.

In 1999, he joined Ingeteam as a Research and Development Engineer in control and regulation for industry, marine, traction, wind, solar, and grid applications. Since 2016, he has been the Research and Development Manager with Ingeteam Power Technology, S.A., and the Managing Director with Ingeteam Research and Development Europe, S.L.